https://lib.uliege.be https://matheo.uliege.be

Final work : Integration scheme of a continuous formulation based on incremental-secant homogenization

Auteur : Pérez Cagegi, Matías Ayrton
Promoteur(s) : Noels, Ludovic
Faculté : Faculté des Sciences appliquées
Diplôme : Master en ingénieur civil en aérospatiale, à finalité spécialisée en "turbomachinery aeromechanics (THRUST)"
Année académique : 2021-2022
URI/URL : http://hdl.handle.net/2268.2/13855

Avertissement à l'attention des usagers :

Tous les documents placés en accès ouvert sur le site le site MatheO sont protégés par le droit d'auteur. Conformément aux principes énoncés par la "Budapest Open Access Initiative"(BOAI, 2002), l'utilisateur du site peut lire, télécharger, copier, transmettre, imprimer, chercher ou faire un lien vers le texte intégral de ces documents, les disséquer pour les indexer, s'en servir de données pour un logiciel, ou s'en servir à toute autre fin légale (ou prévue par la réglementation relative au droit d'auteur). Toute utilisation du document à des fins commerciales est strictement interdite.

Par ailleurs, l'utilisateur s'engage à respecter les droits moraux de l'auteur, principalement le droit à l'intégrité de l'oeuvre et le droit de paternité et ce dans toute utilisation que l'utilisateur entreprend. Ainsi, à titre d'exemple, lorsqu'il reproduira un document par extrait ou dans son intégralité, l'utilisateur citera de manière complète les sources telles que mentionnées ci-dessus. Toute utilisation non explicitement autorisée ci-avant (telle que par exemple, la modification du document ou son résumé) nécessite l'autorisation préalable et expresse des auteurs ou de leurs ayants droit.

University of Liège - School of Engineering and Computer Science

Master's thesis carried out to obtain the degree of Master of Science in Aerospace Engineering

---

Integration scheme of a continuous formulation based on incremental-secant homogenization

---

Author: Matías Ayrton Pérez Cagegi
Tutor: Ludovic Noels
Industry advisor: Samuel Melchior (CENAERO)

Abstract

The field of micromechanics aims to model the behaviour of the continuum of the materials at microscopical level. This work takes a code for a Mean-Field-Homogenization scheme for composite materials and applies a different derivation with the aim of being able to model the continuous reality; to then use a mathematical discretization and be able to draw the stress-strain curve of a number of two-phase composite materials. This model is based on the limit of the classical MFH system of equations to an infinitesimally small time step. This results in a new strain localization tensor that relates the strains in the matrix and inclusion phases, allowing to modify said system and obtain an improved solution.

Wit this new model, one can obtain results with a similar accuracy with respect to the original in one of its variants, the residual-incremental-secant scheme, with a bigger step size in the stress-strain curve. Therefore, the modification of the code performed could be potentially adapted to obtain faster first-order results with an acceptable accuracy.

Acknowledgements

In the first place, I thank my tutor Ludovic Noels for giving me this chance and guiding me in such an important work. Also, to Samuel Melchior for helping me closely, easing the stress with his optimism and making this experience much more enjoyable.

To my parents, for letting me think in my own way and making me who I am today. Without their support I would not have been able to live this experience. They gave me more than I can appreciate right now and I will always be grateful to them.

To all the awesome people I met during the past two years. Sweden and Belgium have been two incredible and very different experiences. I am very glad I could meet so many different people and get to see mentalities and ways of see the world that I could not even start to think of, had I stayed in my hometown. I felt I had two small families that I will forever carry within me. Each taught me different things. I enjoyed every moment with them. I learnt a lot more than I thought I would about people and myself, and this really changed how I want to live my life in the future.

Contents

List of Figures **v**

1 Introduction **1**

2 $\mathbf{J_2}$ elasto-plasticity **7**

2.1 Constitutive Elasto-Plasticity 7

2.2 Radial return mapping 9

2.3 Modified return mapping 12

2.4 Algorithmic operator 15

2.4.1 Algorithmic operator for the radial return mapping 16

2.4.2 Algorithmic operator for the modified return mapping 17

3 Mean-Field Homogenization scheme **19**

3.1 Objectives of the MFH method 19

3.2 The Linear Comparison Composite 21

3.3 Incremental-Secant Scheme 22

3.4 MFH as a material law 26

3.5 Homogenization Resolution 27

4 Continuous formulation **29**

4.1 Derivation of the new localization tensor 29

4.2 MFH system 34

4.3 Constitutive box 35

4.4 Homogenization resolution 36

5 Analysis of the results **39**

5.1 Reliability of the approach 39
5.1.1 Convergence with strain increments 39
5.1.2 Comparison with the residual-incremental formulation when $\Delta\varepsilon \to 0$ 42
5.1.3 Reduced sensitivity to strain increments 42
5.2 Comparison with the results from [1] 43
5.2.1 Case 1 43
5.2.2 Case 2 44
5.2.3 Case 3 45
5.2.4 Case 4 46

6 Conclusions 51

7 Future improvements of the method 53

A Tensor notation 55

B Calculation of the Jacobian for the former incremental-secant method 57

C Components of the Eshelby tensor and their derivatives 59
C.1 Derivative of the Eshelby tensor $\boldsymbol{S}$ 60
C.2 First derivative 60
C.3 Second derivative 61
C.4 Mixed derivative 62

D Derivatives of the shear stiffness μ_r^S 63
D.1 Zero-incremental shear stiffness μ_r^{S0} 63
D.2 Residual-incremental shear stiffness μ_r^{Sr} 63

E Calculation of the Jacobian for the proposed formulation 65

Bibliography 69

List of Figures

1.1 Use of composites in aviation in the past decades. Picture taken from [2]. 2

1.2 Illustration of a composite material. What is called a ply is represented, and a small piece to showcase the microstructure is zoomed in. The two phases, matrix and inclusion, are clearly indicated. Picture taken from [3]. 3

1.3 Zoom to an arbitrary area at a point of integration for a heterogeneous microstructure. Picture taken from [4]. 3

2.1 Separation of the strains in a typical stress-strain curve. Point A presents purely elastic behaviour, whereas B has undergone plasticity. Picture taken from [5]. 8

2.2 Illustration of the radial return mapping. The image shows the classical direction pointing to the origin. Picture taken from [1]. 10

2.3 Illustration of the radial return mapping. The stress and strain tensors at time t_n, as well as the variation in strain, $\Delta\boldsymbol{\varepsilon}$, are known. What is sought with the radial return mapping is the new stress state, $\boldsymbol{\sigma}_{n+1}$. Picture taken from [5] 11

2.4 Unloading performed over a single material. 14

2.5 Illustration of the modified radial return mapping. The image shows the different direction, pointing to the residual stress. Picture taken from [1]. 15

3.1 Stress strain curves comparing both methods at phase level. (a) Shows the Sr method, or residual-incremental-secant. (b) Shows the S0, or zero-incremental-secant method. . 23

4.1 Sensitivity to time steps of the incremental-secant formulation. 29

5.1 Convergence of the CS discretization using C^{Sr}. FE results from *Brassart et al.* [6] . . 40

5.2 Convergence of CS discretization and original formulation with small strain increment. 42

5.3 Sensitivity to strain increments of the CS discretization. Left shows the CS discretization. The figure on the right, the original formulation, ... 43

5.4 Results of case 1. FE from *Jansson* [7]. 44

5.5 Results of case 2. FE from *Doghri et al.* [8]. 45

5.6 Results of case 3. FE from *Wu et al.* [9]. 46

5.7 Results of case 4 (MMC's 1 and 2). FE from *Segurado et al.* [10] and *Pierard et al.* [11]. 48

5.8 Results of case 4 (MMC's 3 and 4). FE from *Brassart et al.* [12]. Experimental data from *Christman et al.* [13]. 49

Chapter 1

Introduction

Be it buildings, bridges or aircraft, one crucial point of an engineer's job is to have an understanding of the forces that interact within a structure. The columns not being thick enough or the momentum over a heavy wing are miscalculated, fatal consequences can occur.

This is where the field of continuum mechanics becomes important. One of its aims is to explain the physical behaviour of solid materials when subject to different forces. Being able to determine the limits of a material in different terms allows not only to push the materials knowing they will not fail. One can then obtain better performance and achieve more efficiency in terms of design, while also improving the safety conditions during operation.

When dealing with complex structures and geometries, the theoretical tools that one has at hand become more complicated to use in an efficient way. This is because at some point, idealizing the whole structure as one block and computing approximations stops being accurate, and more sophisticated methods appear. In particular, the Finite Element Method (FEM) is one of the most popular to make structural analysis.

The main idea is to break down the structure to analyze in several pieces, or "elements" which are connected to each other through boundaryes. Inside each of these elements, the material laws are applied with the given geometry in order to compute the information of that specific element. The delicate point is that the elements have to exchange information to each other in order to accurately represent the problem as a whole. In order to achieve this, a set of boundary conditions is given as input to the problem, as well as the loads that are expected to appear. These boundary conditions are paired with the ordinary or partial differential equations that represent the physics of the problem at hand.

This makes the computation of the problem a matter of solving a large number of equations which depends on the total degrees of freedom of the structure. Each element has its own degrees of freedom based on the characteristics of the problem (it may have an axis fixed, be 2 or 3 dimensional, etc...). The differential equations have to be solved at each of the elements that the structure is broken down into. Inside these elements, there is a known number of integration points, at which the local variables are used to perform a numerical integration. To compute these integrals, a set of boundary conditions and loads, defined by the problem, are needed.

The fact that the integration is numerical instead of analytical means that the FEM computations have a certain accuracy with respect to the real behaviour of the material or structure being tested. Still, FEM analysis is a faster and cheaper way of testing designs before assessing which is the best solution and proceeding with the real world testing.

FEM methods are not new and, in general, the current products offer very accurate results for most of the uses when homogeneous materials are used. However, some industries, specially the aerospace, have been increasing their use of composite materials in the past few years [14], [15], [2].

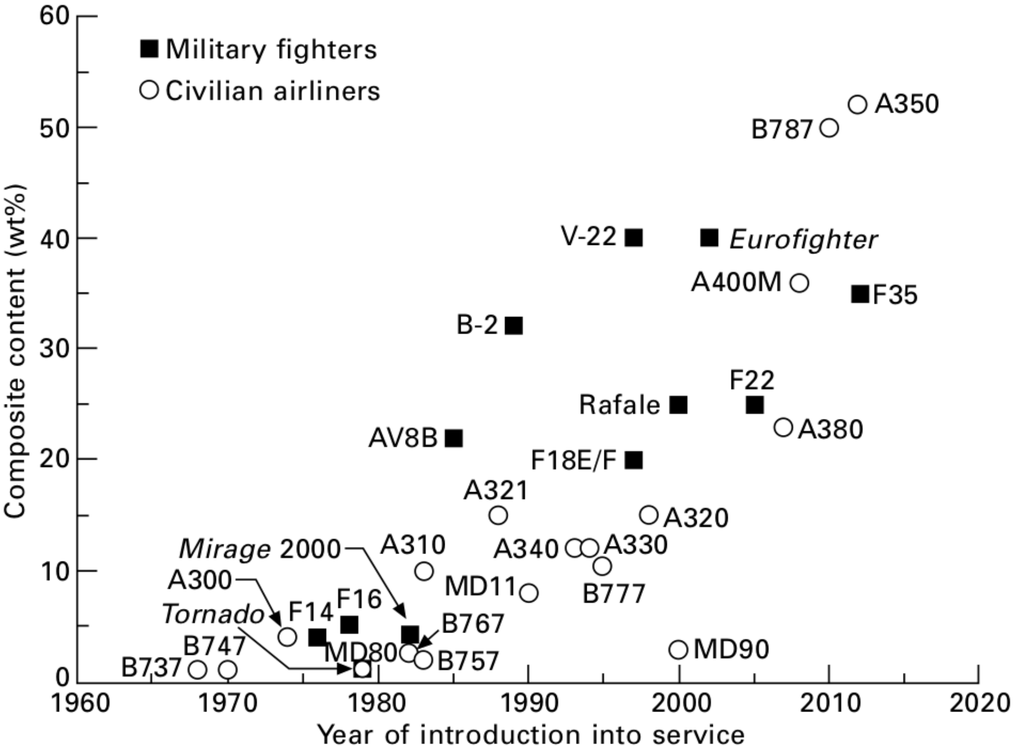

Figure 1.1: Use of composites in aviation in the past decades. Picture taken from [2].

Composite materials are different from commonly used materials in the sense that their microstructure is not homogeneous. Composite materials are constituted by two different materials (also called phases): the material and the inclusions. The inclusions are strong elements whose purpose is to withstand the loads imposed on the composite material. The matrix, on the other hand, is a less resistant element that serves for holding the inclusion phase, protecting the fibre and transmitting the loads to the inclusions.

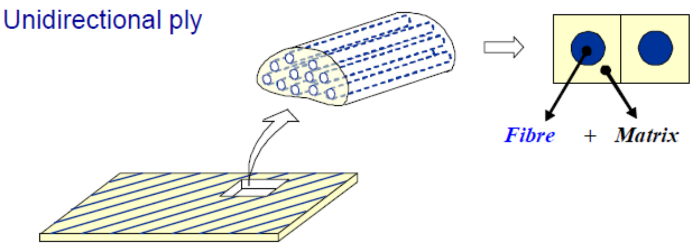

Figure 1.2: Illustration of a composite material. What is called a ply is represented, and a small piece to showcase the microstructure is zoomed in. The two phases, matrix and inclusion, are clearly indicated. Picture taken from [3].

The main advantage of using two different materials is the potential to select each phase in order to taylor the mechanical properties of the resulting composite for a specific application. One of the most common applications in aerospace is to mix a light matrix with an inclusion that is very resistant. The result is a highly resistant material that is at the same time lighter than metal. Some of the most common composites for this applications include Glass Fibre Reinforced Polymers (GFRP) or Carbon Fibre Reinforced Polymers (CFRP). Metal Matrix Composites (MMC) are also very commonly used in a broader field of applications.

On the downside of things, the use of composites also presents a set of drawbacks. Some of them include manufacturing complications, increased complexity of failure mechanics and the fact that composites present anisotropic properties. Under the frame of this project, focus will be made on the fact that the microstructure is inhomogeneous. Figure 1.3 illustrates how the microstructure around an integration point could be when it is taken from a non homogeneous material such as composites. This increased complexity in the material increases the difficulty of computations.

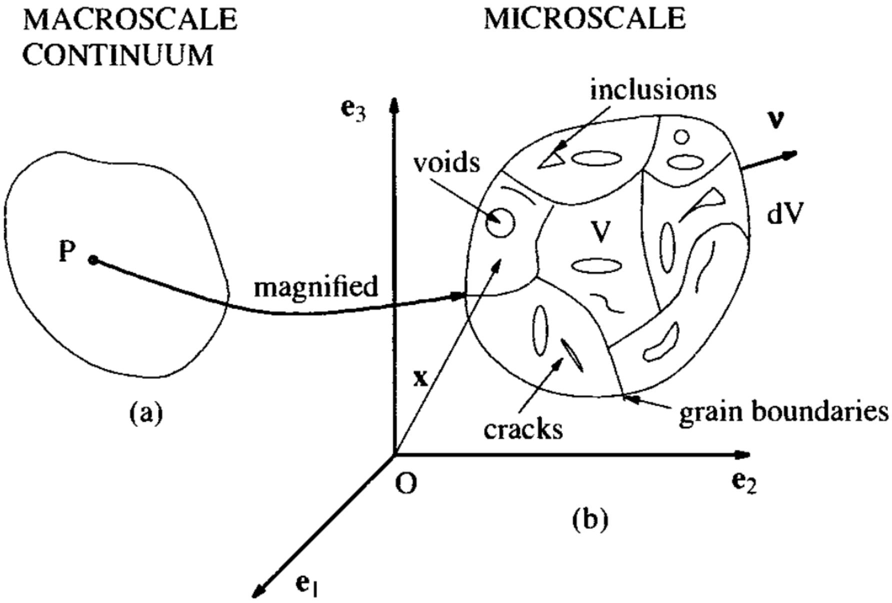

Figure 1.3: Zoom to an arbitrary area at a point of integration for a heterogeneous microstructure. Picture taken from [4].

As mentioned previously, in FEM analysis the integration of the differential equations is performed using local variables at the integration point. However, these local variables are evaluated at the macroscopic level, ranging from a few milimiters up to meters. For the most used metals in aerospace, such as Aluminum or Titanium, it is possible to be accurately modelled with homogeneous mechanical properties. However, for composite materials, the microstructure being heterogeneous means that there must be an information exchange between the two different scales (macroscopic and microscopi), specially in non-linear cases. This depends on the type of the analysis carried out and the complexities that one intends to model and simulate [16], [17]. In the worst cases, the inhomogeneities can make classical FEM analysis have an error of the order of magnitude of 10% or more [18]. The lack of more reliable virtual solutions for the implementation of composite materials makes it necessary to use a lot of physical testing in various phases of the whole process. This is translated to more time and cost.

In order to reduce this error and provide quicker solutions, a number of methods have appeared with the aim of characterizing the composite material and allow a more accurate FEM computation at the macroscopic level. Some methods adapt the FEM to use it to compute the microstructural properties [19], [13], [20]. Other known types include semi-analytical methods; *Kanouté et al.* provide a review of different methods in [21]. Another promising branch of methods is called the homogenization. The method developed in this project falls inside this branch.

The main idea of homogenization is to generate and compute a Representative Volume Element (RVE) around an integration point. This RVE is a portion of the microstructure that serves as a statistical representation of the behaviour at macroscopic scale. The RVE is used to obtain a set of characteristics that can then be used for the FEM formulation. When computing deformations, since the microstructure may vary with load and time, the RVE has to be recomputed whenever there is a change in load at macroscopic level. This defines time or strain increments, depending on if the material is dependent or not on the strain rate. Hence, there is a feedback loop in which the macroscopic FEM solver sends information to the homogenization method, which computes the RVE to be used for the whole model and gives it back to the FEM to perform a new calculation. Ultimately, this results in an iterative procedure that converges on the macroscopic result for the stress-strain relation. it must be noted that computing an RVE is very time consuming so the semi-analytical methods are a way of tackling this setback.

The main pillars for homogenization methods are the Rule of mixtures, relating the stress and strain of the material phases and their volumetric fractions with the stress and strain at the macroscopic level of the composite; and the Eshelby solution [22]. This solution provides a tensor coming from the resolution of the problem of obtaining the strain field around an elastic inclusion in an infinite media. This tensor, along with a number of assumptions on the inclusions interactions allows to obtain models for the microstructure of the RVE. Depending on the model used (such as the Reuss [23], Voigt [24] or the Mori-Tanaka [25]), different expressions are obtained for what is called a strain localization tensor. This tensor relates the strain field in the inclusion with either the strain field of the matrix phase or the macroscopic phase.

The strain localization tensor, along with the rule of mixtures for the stress and strain in the composite allow to write a system of equations that, when solved, gives the macroscopic stress and strain field of the RVE or, in other words, the homogenized characteristics around the integration point for the FEM solver.

What this project aims to achieve is to implement a new formulation, based on the incremental-secant mean-field homogenization (MFH) proposed by *Wu et al.* in [1]. Said paper serves as reference for the present work. The method developed there, which relies on a finite time integration, proved to require a small size of the strain increment (or time step/increment, if the material is strain-rate dependent) in order to reach a converged solution. This leads to the necessity of increasing the number of strain increments used just for the sake of accuracy, which increases the computational time.

The continuous formulation developed herein shows an alternative version of that same code that, in theory, could allow more flexibility in its time integration (methods, size of increments...).

As will be seen in the following chapters, the basis of the new formulation is to develop a new strain localization tensor under the condition that the time increment is infinitesimally small. This will provide an approach different from the original paper's one which, again, could allow for a faster first moment calculation.

Before going into the homogenization methods, the constitutive laws used at component level are detailed in Chapter 2. As mentioned, there are different scales of interest in the whole MFH procedure. The J_2 elasto-plasticity model explained in said chapter is used for each material phase of the composite separately. Most of it rests separatedly from the MFH theory but, in some cases, concepts from MFH are be introduced. These cases have the necessary remark and are explained further in Chapters 3 and the following.

Chapter 3 explains the resolution scheme that was developed by *Wu et al.* in [1], the paper that serves as basis for the present work. The concepts that have been mentioned in the introduction are explained in detail. Furthermore, notation for both macroscopic and microscopic scale is introduced.

After explaining the base formulation, Chapter 4 introduces the proposed one. The main hypothesis for the work is explained and then the new strain localization tensor is developed. Afterwards, the new code (which is the result of a modification of the original) is outlined.

Chapter 5 includes the results of the new formulation. A comparison with the results from both [1] and the very same experiments the paper uses to check its code against is made and partial conclusions are drawn from the results.

Chapters 6 and 7 give closure to the document by assesing the results and the feasibility of the formulation developed, as well as commenting on improvement possibilities to the code that can be introduced in future works.

Chapter 2

J_2 elasto-plasticity

2.1 Constitutive Elasto-Plasticity

The aim of this section is to present the constitutive material laws that are used in the project. These are implemented with the objective of obtaining the stress-strain curve of the phase by computing a set of mechanical states. Each state has a set of properties (such as the internal variables) which can be used to determine the stress when the strain is given. For this, apart from the stress-strain relation itself, the so-called J_2 plasticity theory is used, devised by *von Mises* in [26].

The stress-strain relation in elastic conditions is modelled by Hooke's law for continuous media,

$$\boldsymbol{\sigma} = \boldsymbol{C}^{el} : \boldsymbol{\varepsilon}^{el} \qquad , \tag{2.1}$$

where $\boldsymbol{C}^{el}$ is Hooke's operator. It characterizes the interaction between the stress and strain tensors in elastic conditions.

When there is also plastic deformation, the total strain can be additively decomposed into elastic and plastic parts, as $\boldsymbol{\varepsilon} = \boldsymbol{\varepsilon}^{el} + \boldsymbol{\varepsilon}^{p}$ (for small deformations). When this happens, one can re-write Eq. (2.1) with the elastic strain as a function of the total and plastic ones. This strain separation is easily seen in Figure 2.1.

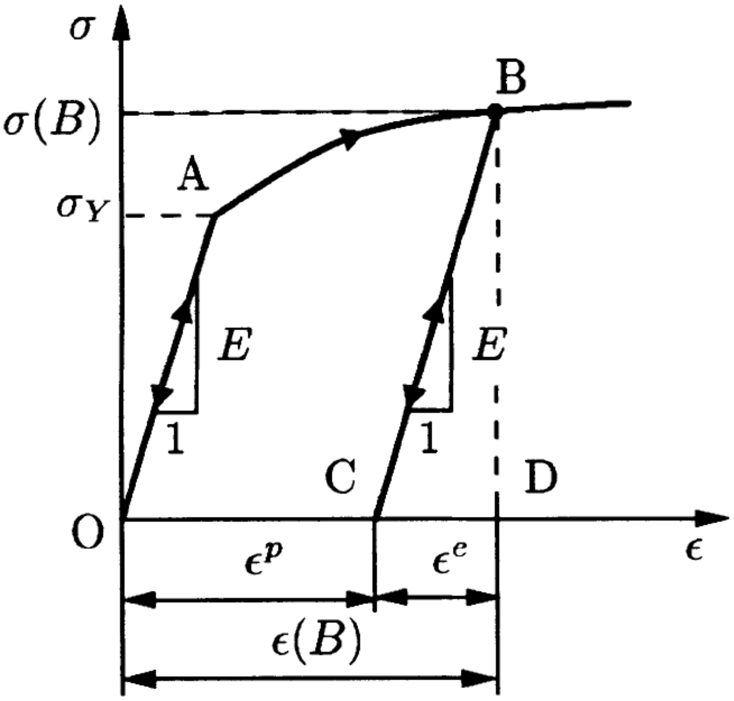

Figure 2.1: Separation of the strains in a typical stress-strain curve. Point A presents purely elastic behaviour, whereas B has undergone plasticity. Picture taken from [5].

Plugging this decomposition into Equation (2.1) yields:

$$\boldsymbol{\sigma} = \boldsymbol{C}^{el} : (\boldsymbol{\varepsilon} - \boldsymbol{\varepsilon}^p) \tag{2.2}$$

The J_2 elasto-plasticity model defines an equivalent stress (the so-called von Mises Stress) to which the material is subjected. This stress is used as an indicator of yielding in said material, by comparing it with the yielding point. The theory defines a "yield surface function" f:

$$f = \sigma^{eq} - \sigma_Y - R(p) \leq 0 \tag{2.3}$$

Here, σ_Y is the initial yield stress of the material, which does not change nor with time nor with stress. $R(p)$ is the hardening model applied, whose expression (and therefore its derivatives) is known and dependent on the accumulated plastic deformation, p. The expression for the equivalent plastic strain is:

$$p(t) = \int_0^t \sqrt{\frac{2}{3}\dot{\boldsymbol{\varepsilon}}^p : \dot{\boldsymbol{\varepsilon}}^p} dt \tag{2.4}$$

The term $\dot{\boldsymbol{\varepsilon}}^p$ is the plastic strain rate, the variation of plastic strain with time. It is modelled by the plastic flow rule:

$$\dot{\boldsymbol{\varepsilon}}^p = \dot{p}\frac{\partial f}{\partial \boldsymbol{\sigma}} \tag{2.5}$$

Here, $\dot{p}$ is the plastic multiplier and it is always equal to or greater than zero. This is defined by the state of the yield function: In elasticity, $\dot{p} = 0$ (plastic strain is not increasing, so p does not vary), whereas $\dot{p} > 0$ in plasticity (p increases, which shows that $\dot{\boldsymbol{\varepsilon}}^p$ is not zero and therefore $\boldsymbol{\varepsilon}^p$ is changing).

Lastly, σ^{eq} is the aforementioned von Mises stress. Its expression reads:

$$\begin{gathered} \sigma^{eq} = \sqrt{\frac{3}{2}\boldsymbol{s} : \boldsymbol{s}} \\ \boldsymbol{s} = \boldsymbol{I}^{dev} : \boldsymbol{\sigma} \end{gathered} \tag{2.6}$$

Here, $\boldsymbol{I}^{dev}$ represents the deviatoric part of the fourth order identity tensor. It is computed as $\boldsymbol{I}^{dev} = \boldsymbol{I} - \frac{1}{3}\boldsymbol{I} \otimes \boldsymbol{I}$.

As said, the von Mises stress is used to evaluate if there is plasticity. In the cases where $f < 0$, one can say that the evaluated state is "inside" the yield surface, and is therefore in elastic state. In the opposite case, there is already plasticity involved. In this model, basically, the equivalent stress cannot be greater than the initial yielding stress plus the hardening in order to avoid plasticity.

The plastic regime introduces some nonlinearities that make it more difficult to compute the stress from a known variation in strain. The next two sections detail how the theory tackles this case.

2.2 Radial return mapping

The so-called radial return mapping allows to construct the stress-strain curve of a material with the stress field being unknown. In order to do this, a different mechanical state, corresponding to a point of the stress-strain curve, is considered at a specific time t_n. With the known input of the strain change from t_n to the next point t_{n+1}, $\Delta\boldsymbol{\varepsilon}_{n+1}$, one can use the method here explained to obtain the stress at t_{n+1} or, in other words, update the stress field. Doing this iteratively, one can compute the curve step by step

For the radial return mapping, a very important concept is needed, called the plastic flow direction. It is the derivative of the yield function as a function of the stress, $\dfrac{\partial f}{\partial \sigma}$. The plastic flow direction is commonly indicated as $\boldsymbol{N}$. Its expression is given by:

$$\boldsymbol{N}_{n+1} = \frac{3}{2}\frac{\boldsymbol{I}^{dev} : \boldsymbol{\sigma}_{n+1}}{\sigma^{eq}_{n+1}} \tag{2.7}$$

This direction is normally pointing to the origin of the stress space, as seen in Figure 2.2. It is worth noting that this quantity is defined also for the elastic region, indicating the possible direction in case there were plasticity. This quantity is, however, not used in such cases.

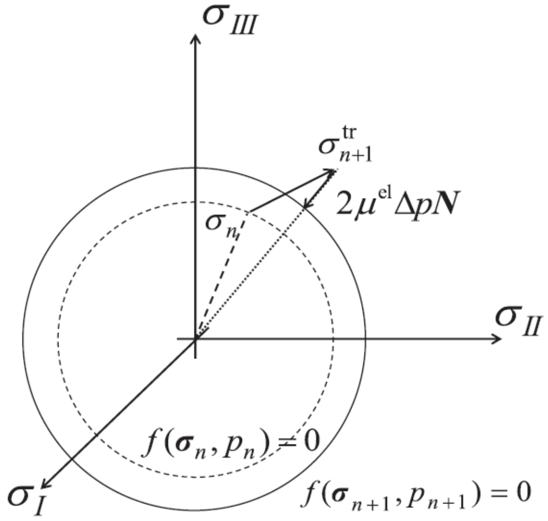
σ_{III}
σ^{tr}_{n+1}
$2\mu^{el}\Delta p\boldsymbol{N}$
σ_n
σ_{II}
$f(\boldsymbol{\sigma}_n, p_n) = 0$
σ_I
$f(\boldsymbol{\sigma}_{n+1}, p_{n+1}) = 0$

Figure 2.2: Illustration of the radial return mapping. The image shows the classical direction pointing to the origin. Picture taken from [1].

Pursuing the objective of updating the stress field, the trial stress $\boldsymbol{\sigma}^{tr}_{n+1}$ is defined. This is a guess on what the stress will be when the updated strain field is applied; to be corrected using a predictor-corrector method. The trial stress is assumed to follow an elastic behaviour, i.e.,

$$\boldsymbol{\sigma}^{tr}_{n+1} = \boldsymbol{\sigma}_n + \boldsymbol{C}^{el} : \Delta\boldsymbol{\varepsilon}_{n+1} \tag{2.8}$$

Therefore, the stress in the updated mechanical state is equal to the stress in the previous onem plus the change produced by the applied strain field. The trial stress can also be used to define a trial plastic flow direction, $\boldsymbol{N}^{tr}$.

$$\boldsymbol{N}^{tr}_{n+1} = \frac{3}{2}\frac{\boldsymbol{I}^{dev} : \boldsymbol{\sigma}^{tr}_{n+1}}{\left(\sigma^{tr}_{n+1}\right)^{eq}} \tag{2.9}$$

Figure 2.3 shows the interpretation of the general guess on the stress-strain curve.

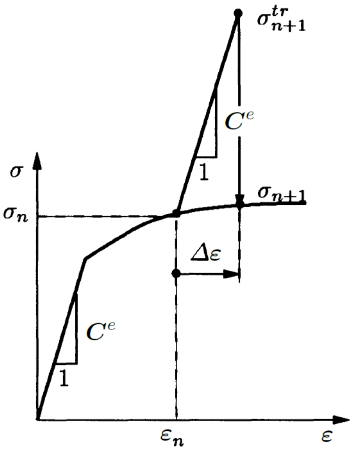

Figure 2.3: Illustration of the radial return mapping. The stress and strain tensors at time t_n, as well as the variation in strain, $\Delta\boldsymbol{\varepsilon}$, are known. What is sought with the radial return mapping is the new stress state, $\boldsymbol{\sigma}_{n+1}$. Picture taken from [5]

The yield condition in Equation (2.3) is tested with the obtained trial stress. If the material is under elasticity, the trial stress is confirmed to be the correct one and the next mechanical state can be evaluated. Clearly the interest of this method is to compute the stress when outside the elastic region, therefore, **plasticity will be assumed during the rest of the chapter**. It is important to clarify this, as some equations (e.g. Equation (2.14)) make sense under plasticity conditions.

When the material is under plasticity, the plastic corrector is used to calculate the updated stress. With this correction, the trial point is projected over the closest point of the yield surface. Due to hardening, this yield surface may vary from one time step to the next one, so the point is projected over the yield surface at t_{n+1}. The correction yields:

$$\boldsymbol{\sigma}_{n+1} = \boldsymbol{\sigma}^{tr}_{n+1} - \boldsymbol{C}^{el} : \Delta p \boldsymbol{N}_{n+1} \tag{2.10}$$

Where Δp is the variation in accumulated plastic deformation from time t_n to time t_{n+1}, such that $\Delta p = p_{n+1} - p_n$.

Since the yield criterion used is isotropic, $\boldsymbol{C}^{el}$ can be also be assumed to be isotropic. This allows to write $\boldsymbol{C}^{el} = 3\kappa^{el}\boldsymbol{I}^{vol} + 2\mu^{el}\boldsymbol{I}^{dev}$, with μ^{el} the elastic shear stiffness of the material and κ^{el} the elastic bulk modulus. Furthermore, the trace of the updated stress is the same as the trace of the trial stress, so that one can write simply the deviatoric part of both of them (if $\boldsymbol{N}$ is deviatoric). Furthermore, if $\boldsymbol{N}$ is deviatoric, one can write $\boldsymbol{C}^{el} : \boldsymbol{N} = 2\mu^{el}\boldsymbol{N}$. Modifying Equation (2.10):

$$\boldsymbol{s}_{n+1} = \boldsymbol{s}^{tr}_{n+1} - 2\mu^{el}\Delta p \boldsymbol{N}_{n+1} \tag{2.11}$$

One can also input Equation (2.7), both for the stress and trial stress.

$$\frac{2}{3}\boldsymbol{N}_{n+1}\sigma_{n+1}^{eq} = \frac{2}{3}\boldsymbol{N}_{n+1}^{tr}\left(\boldsymbol{\sigma}_{n+1}^{tr}\right)^{eq} - 2\mu^{el}\Delta p\boldsymbol{N}_{n+1} \tag{2.12}$$

Since the plastic flow direction has its module normalized and, by Equation (2.12), they have the same direction, it is deduced that: $\boldsymbol{N} = \boldsymbol{N}^{tr}$. This allows to cancel it out and write:

$$(\boldsymbol{\sigma}_{n+1})^{eq} = \left(\boldsymbol{\sigma}_{n+1}^{tr}\right)^{eq} - 3\mu^{el}\Delta p \tag{2.13}$$

Lastly, the yield function is evaluated at this updated stress in order to have a system of two equations with two unknowns:

$$(\boldsymbol{\sigma}_{n+1})^{eq} - \sigma_Y - R(p) = 0 \tag{2.14}$$

Equations (2.13) and (2.14) can be solved in a system in order to obtain the updated stress, $(\boldsymbol{\sigma}_{n+1})^{eq}$, and the change in plastic deformation, Δp[1]. The full stress field can then be obtained from the equivalent stress by means of the plastic flow direction.

2.3 Modified return mapping

The radial return mapping presented in the previous section shall also be modified for the present work. In the Mean-Field Homogenization scheme that is proposed here, the updated stress is calculated not directly from the previous state at t_n, but rather from a residual stress state. This raises the need for the use of a different operator that is not the elastic one, $\boldsymbol{C}^{el}$. In order for this operator to be isotropic, the modified return mapping described in this section has to be used.

The mentioned residual stress state corresponds to a virtual unloading performed at the mechanical state at t_n. This unloading is elastic, and thus the following is defined:

$$\boldsymbol{\sigma}_n^{res} = \boldsymbol{\sigma}_n - \boldsymbol{C}^{el} : \Delta\boldsymbol{\varepsilon}_n^u \qquad , \tag{2.15}$$

where $\Delta\boldsymbol{\varepsilon}^u$ is the so-called unloading strain, which is commonly defined inside the frame of the MFH scheme. The main interest of this unloading strain is the fact that, if defined, the operator $\boldsymbol{C}^{Sr}$ does not need to be isotropized and can therefore be used for the yield criteria as is, making computations much easier. This operator is explained few paragraphs below.

A new stress increment can be defined with the superscript r, indicating the variation from the residual state to the new mechanical state (as opposed to the change from the previous loaded state to the updated one):

---

[1] Its derivatives are reported in Section 2.4.

$$\Delta \boldsymbol{\sigma}_{n+1}^{r} = \boldsymbol{\sigma}_{n+1} - \boldsymbol{\sigma}_{n}^{res} \tag{2.16}$$

In the same fashion, the residual strain increment relating both states is:

$$\Delta \boldsymbol{\varepsilon}_{n+1}^{r} = \boldsymbol{\varepsilon}_{n+1} - \boldsymbol{\varepsilon}_{n}^{res} \tag{2.17}$$

The introduced residual stress state can be related to the updated load state through the use of the so-called incremental-secant operator. More detail on this is be given in Section 3.3. Nevertheless, the expression for the stress at time t_{n+1} is given in Equation (2.18), showcasing the use of the incremental-secant operator.

$$\boldsymbol{\sigma}_{n+1} = \boldsymbol{\sigma}_{n}^{res} + \boldsymbol{C}^{Sr} : \Delta \boldsymbol{\varepsilon}_{n+1}^{r} \qquad , \tag{2.18}$$

where $\boldsymbol{C}^{Sr}$ is the incremental-secant operator and relates the two mechanical states as given here. Because of the modification of the radial return mapping applied, another definition for this operator is $\boldsymbol{C}^{Sr} = 3\kappa^{el}\boldsymbol{I}^{vol} + 2\mu^{S}\boldsymbol{I}^{dev}$. One can use this expression because the newly introduced operator is isotropic, thanks to the unloading step performed. Again, κ^{el} is the elastic bulk modulus, which is constant under the J_2 plasticity frame; and μ^{S} is the so-called secant shear stiffness, defined in Equations (3.16) and (3.17). Once more, this falls under the frame of MFH, so it is be explained further in Chapter 3.

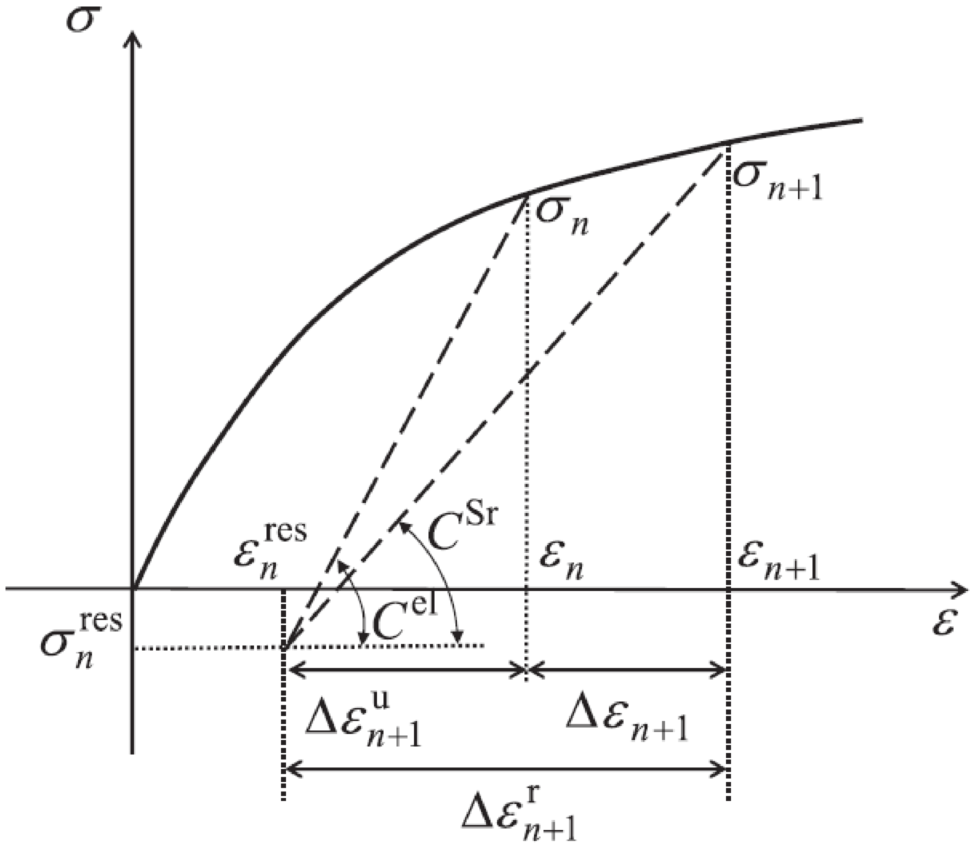

σ
σ_{n+1}
σ_n
C^{Sr}
$\varepsilon_n^{\mathrm{res}}$
ε_n
ε_{n+1}
σ_n^{res}
C^{el}
ε
$\Delta\varepsilon_{n+1}^{\mathrm{u}}$
$\Delta\varepsilon_{n+1}$
$\Delta\varepsilon_{n+1}^{\mathrm{r}}$

Figure 2.4: Unloading performed over a single material.

Coming back to the modified return mapping, since the trial stress is now being added from a different position in the stress space, a new definition is needed for this increment:

$$\Delta\boldsymbol{\sigma}_{n+1}^{tr} = \boldsymbol{\sigma}_{n+1}^{tr} - \boldsymbol{\sigma}_n^{res} \tag{2.19}$$

The plastic flow direction must also be re-written:

$$\boldsymbol{N}_{m,n+1} = \frac{3}{2}\frac{\boldsymbol{I}^{dev} : \Delta\boldsymbol{\sigma}_{n+1}^{r}}{\left(\Delta\boldsymbol{\sigma}_{n+1}^{r}\right)^{eq}} \tag{2.20}$$

The trial plastic flow direction can also be re-written as:

$$\boldsymbol{N}_{m,n+1}^{tr} = \frac{3}{2}\frac{\boldsymbol{I}^{dev} : \Delta\boldsymbol{\sigma}_{n+1}^{tr}}{\left(\Delta\boldsymbol{\sigma}_{n+1}^{tr}\right)^{eq}} = \frac{3}{2}\frac{\boldsymbol{I}^{dev} : \left(\boldsymbol{C}^{el} : \Delta\boldsymbol{\varepsilon}_{n+1}^{r}\right)}{\left(\boldsymbol{C}^{el} : \Delta\boldsymbol{\varepsilon}_{n+1}^{r}\right)^{eq}} \tag{2.21}$$

As opposed to Figure 2.2, the direction is now pointing to the residual stress in the stress space, instead of the origin. This is illustrated by Figure 2.5.

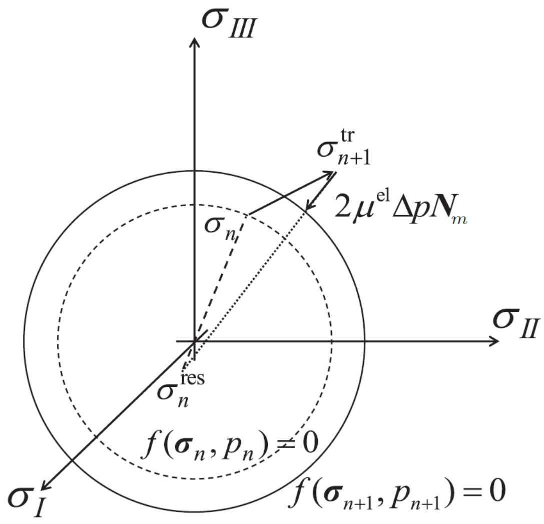
σ_{III}
$\sigma_{n+1}^{\mathrm{tr}}$
$2\mu^{\mathrm{el}}\Delta p\boldsymbol{N}_m$
σ_n
σ_{II}
σ_n^{res}
$f(\boldsymbol{\sigma}_n, p_n) = 0$
σ_I
$f(\boldsymbol{\sigma}_{n+1}, p_{n+1}) = 0$

Figure 2.5: Illustration of the modified radial return mapping. The image shows the different direction, pointing to the residual stress. Picture taken from [1].

Following the same procedure as with the regular radial return mapping yields the following system:

$$\begin{cases} (\boldsymbol{\sigma}_{n+1} - \boldsymbol{\sigma}_n^{res})^{eq} + 3\mu^{el}\Delta p = \left(\boldsymbol{\sigma}_{n+1}^{tr} - \boldsymbol{\sigma}_n^{res}\right)^{eq} \\ (\boldsymbol{\sigma}_{n+1})^{eq} - \sigma_Y - R(p_{n+1}) = 0 \end{cases} \tag{2.22}$$

This gives approximations of the updated stress and accumulated plastic deformation when one parts from the residual stress state.

2.4 Algorithmic operator

The so-called algorithmic operator allows to define slight variations around the stress and strain fields and improve convergence and accuracy. This is in turn solved globally using the Jacobian matrix. The algorithmic operator is defined as:

$$\delta\boldsymbol{\sigma} = \boldsymbol{C}^{alg} : \delta\boldsymbol{\varepsilon} \tag{2.23}$$

Two different algorithmic tangent operators can be defined, depending on the return mapping algorithm used. The algorithmic operator is always computed at the new time step, thus, at t_{n+1}. This subscript has been omitted in this section, since the expressions for $\boldsymbol{C}^{alg}$ are all evaluated at t_{n+1}.

2.4.1 Algorithmic operator for the radial return mapping

If one considers the updated and corrected stress given in Equation (2.10), the expression for the algorithmic operator can be derived. As a first step, taking derivatives with respect to the strain yields:

$$\boldsymbol{C}^{alg} = \frac{\partial \boldsymbol{\sigma}^{tr}}{\partial \boldsymbol{\varepsilon}} - \boldsymbol{C}^{el} : \left[\boldsymbol{N} \otimes \frac{\partial \Delta p}{\partial \boldsymbol{\varepsilon}} + \Delta p \frac{\partial \boldsymbol{N}}{\partial \boldsymbol{\varepsilon}} \right] \tag{2.24}$$

From the definition of the trial stress, its derivative is straightforward:

$$\frac{\partial \boldsymbol{\sigma}^{tr}}{\partial \boldsymbol{\varepsilon}} = \boldsymbol{C}^{el} \tag{2.25}$$

The derivative of the plastic strain increment, Δp, can be obtained by combining Equations (2.13) and (2.14). The definition of the equivalent stress given by the former can be introduced into the latter to give:

$$\left(\boldsymbol{\sigma}^{tr}\right)^{eq} - 3\mu^{el} \Delta p - \sigma_Y - R(p) = 0 \tag{2.26}$$

Taking derivatives with respect to the strain yields

$$\frac{\partial \left(\boldsymbol{\sigma}^{tr}\right)^{eq}}{\partial \boldsymbol{\varepsilon}} - 3\mu^{el} \frac{\partial \Delta p}{\partial \boldsymbol{\varepsilon}} - \frac{dR}{dp} \frac{\partial p}{\partial \boldsymbol{\varepsilon}} = 0 \qquad , \tag{2.27}$$

where the derivative of the equivalent trial stress reads:

$$\frac{\partial \left(\boldsymbol{\sigma}^{tr}\right)^{eq}}{\partial \boldsymbol{\varepsilon}} = \boldsymbol{N} : \boldsymbol{I}^{dev} : \boldsymbol{C}^{el} = 2\mu^{el} \boldsymbol{N} \tag{2.28}$$

The variation of the yield stress is 0 with respect to the strains. Furthermore, the variations of Δp and p are equivalent, so that one can take them out as common factor when differentiated. Rearranging:

$$\frac{\partial \Delta p}{\partial \boldsymbol{\varepsilon}} = \frac{1}{3\mu^{el} + \frac{dR}{dp}} \boldsymbol{N} : \boldsymbol{I}^{dev} : \boldsymbol{C}^{el} = \frac{2\mu^{el}}{h} \boldsymbol{N} \tag{2.29}$$

Here, the term $h = 3\mu^{el} + \dfrac{dR}{dp}$, which is commonly used, is introduced. The equality $\boldsymbol{C}^{el} : \boldsymbol{I}^{dev} = 2\mu^{el} \boldsymbol{I}^{dev}$ is also used to further simplify the expression. Moreover, since $\boldsymbol{N}$ is deviatoric, multiplying it by $\boldsymbol{I}^{dev}$ yields $\boldsymbol{N}$.

Continuing, the derivative of the classical plastic flow direction is

$$\frac{\partial \boldsymbol{N}}{\partial \boldsymbol{\varepsilon}} = \frac{2\mu^{el}}{(\boldsymbol{\sigma}^{tr})^{eq}} \left[\frac{3}{2}\boldsymbol{I}^{dev} - \boldsymbol{N} \otimes \boldsymbol{N}\right] \tag{2.30}$$

Finally, introducing Equations (2.25), (2.29), and (2.30) into (2.24) yields:

$$\boldsymbol{C}^{alg} = \boldsymbol{C}^{el} - \frac{1}{h}\boldsymbol{C}^{el} : \boldsymbol{N} \otimes \boldsymbol{I}^{dev} : \boldsymbol{C}^{el} : \boldsymbol{N} - \frac{\left(2\mu^{el}\right)^2 \Delta p}{(\boldsymbol{\sigma}^{tr})^{eq}} \left(\frac{3}{2}\boldsymbol{I}^{dev} - \boldsymbol{N} \otimes \boldsymbol{N}\right) \tag{2.31}$$

Here, one can again make use of the equality $\boldsymbol{C}^{el} : \boldsymbol{I}^{dev} = 2\mu^{el} : \boldsymbol{I}^{dev}$ to simplify the expression. Therefore, the final expression is obtained:

$$\boldsymbol{C}^{alg} = \boldsymbol{C}^{el} - \frac{\left(2\mu^{el}\right)^2}{h} (\boldsymbol{N} \otimes \boldsymbol{N}) - \frac{\left(2\mu^{el}\right)^2 \Delta p}{(\boldsymbol{\sigma}^{tr})^{eq}} \left(\frac{3}{2}\boldsymbol{I}^{dev} - \boldsymbol{N} \otimes \boldsymbol{N}\right) \tag{2.32}$$

Note again that this algorithmic operator is only correctly defined for the classical radial return mapping. In the case of the modified return mapping, a new definition is needed due to the changes in the plastic flow direction.

2.4.2 Algorithmic operator for the modified return mapping

For this method, the initial point is

$$\boldsymbol{\sigma} = \boldsymbol{\sigma}^{tr} - \boldsymbol{C}^{el} : \Delta p \boldsymbol{N}_m \qquad , \tag{2.33}$$

which leads after differentiating to

$$\boldsymbol{C}_m^{alg} = \frac{\partial \boldsymbol{\sigma}^{tr}}{\partial \boldsymbol{\varepsilon}} - \boldsymbol{C}^{el} : \left[\boldsymbol{N}_m \otimes \frac{\partial \Delta p}{\partial \boldsymbol{\varepsilon}} + \Delta p \frac{\partial \boldsymbol{N}_m}{\partial \boldsymbol{\varepsilon}}\right]. \tag{2.34}$$

The process to obtain the derivative of the plastic deformation starts now with the equation defining the yield surface.

$$(\boldsymbol{\sigma}_{n+1})^{eq} - \sigma_Y - R(p) = 0 \tag{2.35}$$

Taking derivatives with respect to the stress gives:

$$\frac{\partial\left(\boldsymbol{\sigma}_{n+1}\right)^{eq}}{\partial\boldsymbol{\sigma}} = \frac{dR}{dp}\frac{\partial p}{\partial\boldsymbol{\sigma}} = \boldsymbol{N} \tag{2.36}$$

Multiplying on both sides by $\dfrac{d\boldsymbol{\sigma}}{d\boldsymbol{\varepsilon}}$ yields:

$$\frac{\partial\left(\boldsymbol{\sigma}_{n+1}\right)^{eq}}{\partial\boldsymbol{\varepsilon}} = \frac{dR}{dp}\frac{\partial p}{\partial\boldsymbol{\varepsilon}} = \boldsymbol{N} : \left[\boldsymbol{C}^{el} - \boldsymbol{C}^{el} : \left(\boldsymbol{N}_m \otimes \frac{\partial\Delta p}{\partial\boldsymbol{\varepsilon}} + \Delta p\frac{\partial\boldsymbol{N}_m}{\partial\boldsymbol{\varepsilon}}\right)\right] \tag{2.37}$$

$\dfrac{\partial\Delta p}{\partial\boldsymbol{\varepsilon}}$ can be factored out, obtaining a final expression for it:

$$\frac{\partial\Delta p}{\partial\boldsymbol{\varepsilon}} = \frac{2\mu^{el}}{h_m}\boldsymbol{N} - \frac{2\mu^{el}\Delta p}{h_m}\boldsymbol{N} : \frac{\partial\boldsymbol{N}_m}{\partial\boldsymbol{\varepsilon}} \tag{2.38}$$

where $h_m = 2\mu^{el}\boldsymbol{N}_m : \boldsymbol{N} + \dfrac{dR}{dp}$.

The last derivative needed to evaluate Equation (2.34) is that of the modified plastic flow direction,

$$\frac{\partial\boldsymbol{N}_m}{\partial\boldsymbol{\varepsilon}} = \frac{2\mu^{el}}{\left(\Delta\boldsymbol{\sigma}^{tr}\right)^{eq}}\left[\frac{3}{2}\boldsymbol{I}^{dev} - \left(\boldsymbol{N}_m \otimes \boldsymbol{N}_m\right)\right]. \tag{2.39}$$

Now, one can input Equations (2.25), (2.38) and (2.39) into Equation (2.34) and obtain the final expression:

$$\boldsymbol{C}_m^{alg} = \boldsymbol{C}^{el} - \frac{\left(2\mu^{el}\right)^2}{h_m}\left(\boldsymbol{N}_m \otimes \boldsymbol{N}\right) + \left[\frac{\left(2\mu^{el}\right)^2\Delta p}{\left(\Delta\boldsymbol{\sigma}^{tr}\right)^{eq}}\left(\frac{2\mu^{el}}{h_m}\left(\boldsymbol{N}_m \otimes \boldsymbol{N}\right) + \boldsymbol{I}\right)\right]\left(\frac{3}{2}\boldsymbol{I}^{dev} - \boldsymbol{N}_m \otimes \boldsymbol{N}_m\right) \tag{2.40}$$

Chapter 3

Mean-Field Homogenization scheme

This chapter summarizes the main points of the resolution scheme developed by *Wu et al.* in [1], which is be compared to the present one afterwards.

3.1 Objectives of the MFH method

The final goal is to, as said, obtain the macroscopic stress at the next time step in order to build the full stress-strain curve and characterize the material while considering the micro-structure of both phases. The calculations are performed by a code in C, developed at University of Liège.

First, the idea of how the code solves the problem is recalled. The stress-strain curve is built by obtaining the mechanical state at each point of the curve, with the updated strain field known as an input. This means that a number of points have to be calculated. In each of them, a value of the macroscopic $\Delta\bar{\varepsilon}_{n+1}$ is given. This value is used to compute the values of stress and strain at microstructural level (i.e., values from each material phase). After a homogenized macroscopic stress value is obtained using the microstructure, this one is used to solve the FEM boundary value problem at macroscopic level. This requires an iterative procedure on $\Delta\bar{\varepsilon}_{n+1}$, that is updated and sent back to the homogenization procedure once more if the macroscopic FEM has not converged. New and more accurate material phase magnitudes are computed and then a new macroscopic stress value is computed to be fed again to the FEM code.

In general,the points of the stress-strain curve are separated by "time steps", or Δt. One wants to calculate the next point of the curve. The previous time step is regarded as t_n and, the one of interest, t_{n+1}, also called current time step. It must be noted that this nomenclature makes sense mostly for cases with strain-rate dependency, such as elasto-viscoplastic materials.

In the cases in which the time dependency is not important, the different time steps could still indicate points in the curve. These points are distinct points that represent all the mechanical states. However, for the sake of being clear, istead of time steps, the variation from one mechanical state to another is measured in in strain increments whenever the cas is not strain-rate dependent.

As said, for each of these mechanical states, the J_2 plasticity model is applied to each phase and afterwards a set of equations is solved. The full resolution of the equations gives the updated macroscopic stress at the end of the time step or strain increment consider considered, i.e., at t_{n+1}. For linear cases, the system reads:

$$\begin{cases} \bar{\boldsymbol{\varepsilon}} = v_0 \boldsymbol{\varepsilon}_0 + v_I \boldsymbol{\varepsilon}_I \\ \bar{\boldsymbol{\sigma}} = v_0 \boldsymbol{\sigma}_0 + v_I \boldsymbol{\sigma}_I \end{cases} \tag{3.1}$$

$$\boldsymbol{\varepsilon}_I = \boldsymbol{B}\left(\boldsymbol{C}_0^{el}, \boldsymbol{C}_I^{el}\right) : \boldsymbol{\varepsilon}_0 \tag{3.2}$$

$$\boldsymbol{B}\left(\boldsymbol{C}_0^{el}, \boldsymbol{C}_I^{el}\right) = \left\{\boldsymbol{I} + \boldsymbol{S}\left(\boldsymbol{C}_0^{LCC}\right) : \left[\left(\boldsymbol{C}_0^{el}\right)^{-1} : \boldsymbol{C}_I^{el} - \boldsymbol{I}\right]\right\}^{-1} \tag{3.3}$$

The two first equations are the rule of mixtures. They allow to compute the averaged stress and strain over the RVE with the information of both material phases. The subscripts "I" and "0" stand for the inclusion and matrix phases, respectively. As an example, v_I and v_0 refer to the volumetric fraction of inclusion and matrix phase, respectively.

The bar notation introduced over the strains and stresses is commonly used in the frame of homogenization. It indicates that a tensor or quantity is defined uniformly over its phase. For the present work, the bar is used mostly to refer to the composite level, meaning that it is an average value over it. The absence of both bar and subscript means that the magnitudes can refer to either the composite or the phase level. Also, subscript "r" is used to refer to a generic material phase, such that it can be substituted by either I or 0.

The last two are related to the so-called strain localization tensor[1], $\boldsymbol{B}$. As it can be seen, this invertible tensor relates the variation in strain in the matrix to the one in the inclusions, allowing to directly compute the average over the RVE once one of the two phase strains is known.

The expression for the localization tensor, given in Equation (3.3), comes from the so-called Mori-Tanaka (or simply MT) scheme developed by *Mori and Tanaka* in [25]. This is one way of computing the strain localization tensor that, as shown by *Wu et al.* in [1], gives good results when it is applied to two-phase composites. Since it is used in the reference paper and thus implemented in the code, the MT scheme is utilized for the present work.

The tensor $\boldsymbol{S}$ appearing in this expression is the so-called Esheelby tensor that was mentioned in the introduction. Again, it is coming from the fundamental solution of [22] and its expression depends on the geometrical properties of the inclusion phase (shape, aspect ratio). For the case being, its expression can be found in Appendix C.

---

[1] Another strain localization tensor is commonly defined defined and, in fact, is also used in the code developed before this work. This tensor is called **A** and relates the strains in the inclusion to the strains in the RVE. It is introduced in Section 3.4.

To close the system of equations, Hooke's law can be used for each phase. Since this Section considers only the elastic case, one has:

$$\boldsymbol{\sigma}_r = \boldsymbol{C}^{el} : \boldsymbol{\varepsilon}_r \tag{3.4}$$

Lastly, an important assumption is that the macro-scale strain obtained from the FEM is constant over the RVE[2]. This can only be applied if the representative lengths of the macro-scale, micro-scale and the RVE are separated well enough. As stated by *Noels* [29], the assumption of the macro-scale strain being constant over the RVE holds if:

$$l_M >> l_{VE} >> l_m \tag{3.5}$$

Note that the present method only uses teh macroscopic and microscopic scale, so that l_{VE} is not used here.

3.2 The Linear Comparison Composite

There are cases in which the behaviour of a material is not linear, such as with composites. For such cases, the concept of a Linear Comparison Composite (LCC) is introduced.

The idea behind the LCC is to linearize the local response over the RVE in a macroscopic point. This linearization is valid only for a finite time step, meaning that the LCC has to be re-defined at each point of the stress-strain curve. This way, one can obtain a stress-strain relation that is linear, but can be used to approximate the actual non-linear behaviour. Different methods can be used to define different LCC's, which modify the operator used in Equation (2.1) (whenever the case is non-linear, s.t. one does not have only $\boldsymbol{\varepsilon}^{el}$ on the RHS).

The definition of this new operator, called $\boldsymbol{C}^{LCC}$ generically, allows to approximate the material's stress-strain curve by linearizing each point of the curve. Different methods that are explained for example by *Brassart* in [30] define a variety of operators that are used to obtain this curve. In general, one is always interested in how an input in the strain is going to affect the stress over the RVE, following the interaction given by $\boldsymbol{C}^{LCC}$. This operator varies over the stress-strain curve, so it has to be recalculated for each mechanical state.

The use of the Linear Comparison Composite allows to write the strain localization tensor as a function of the new operator:

$$\Delta\boldsymbol{\varepsilon}_I = \boldsymbol{B}\left(\boldsymbol{C}_0^{LCC}, \boldsymbol{C}_I^{LCC}\right) : \Delta\boldsymbol{\varepsilon}_0 \tag{3.6}$$

---

[2] This assumption of homogeneity over the RVE might not hold near regions with high gradients such as free edges or macroscopic cracks, as mentioned in [27] or [28]. Still, addressing the impact of this assumption on the results is not the scope of this work.

$$\boldsymbol{B}\left(\boldsymbol{C}_0^{LCC},\boldsymbol{C}_I^{LCC}\right)=\left\{\boldsymbol{I}+\boldsymbol{S}\left(\boldsymbol{C}_0^{LCC}\right):\left[\left(\boldsymbol{C}_0^{LCC}\right)^{-1}:\boldsymbol{C}_I^{LCC}-\boldsymbol{I}\right]\right\}^{-1} \tag{3.7}$$

As said, the LCC is a construct that allows to linearize the non-linear behaviour of the real material. Different LCC's can be defined depending on the method one has developed. In the present work, the so-called incremental-secant method is used as basis. This method is explained in the next section.

3.3 Incremental-Secant Scheme

The aforementioned incremental-secant method is a way of defining a Linear Comparison Composite that relies on the use of finite time steps. These time steps introduce in turn finite strain and stress differences in the formulation. From now onwards, the LCC operator will be indicated as $\boldsymbol{C}^S$ because it is now particularized to secant methods.

In order to define incremental schemes, a virtual unloaded state is defined. In this state, the residual stresses and strains are introduced ($\boldsymbol{\sigma}_n^{res}$ and $\boldsymbol{\varepsilon}_n^{res}$, respectively). In this unloaded state, the composite sees no residual stress by definition, which is translated to imposing:

$$\bar{\boldsymbol{\sigma}}_n^{res}=v_0\boldsymbol{\sigma}_{0,n}^{res}+v_I\boldsymbol{\sigma}_{I,n}^{res}=0 \tag{3.8}$$

Where v_0 and v_I are the volume fraction in the matrix and inclusion phases, respectively.

This gives an extra equation to be used with the system of equations to solve for the MFH. Apart from $\bar{\boldsymbol{\sigma}}_n^{res}$ being 0, the residual stresses at phases, as well as the residual strains at all levels (both phase and composite) might be very well expected to be different from 0. They need therefore to be calculated.

In order to do so, at each time step, the LCC undergoes a virtual, elastic unloading. This unloading moves the state from the considered mechanical state (either at time t_n or t_{n+1}) to a residual stress state. Again, the objective of this unloading is to obtain a zero residual stress over the whole composite.

The unloading is always performed using the elastic operator $\boldsymbol{C}^{el}$, thus, the unloading strain (indicated by $\boldsymbol{\varepsilon}_n^u$) varies slightly along the stress-strain curve. Even so, it must still be recomputed at each time step.

The representation of the unloading can be seen in Figure 3.1 at time t_n. The line with the slope defined by $\boldsymbol{C}^{el}$ goes from $\boldsymbol{\varepsilon}_n$ to $\boldsymbol{\varepsilon}_n^{res}$.

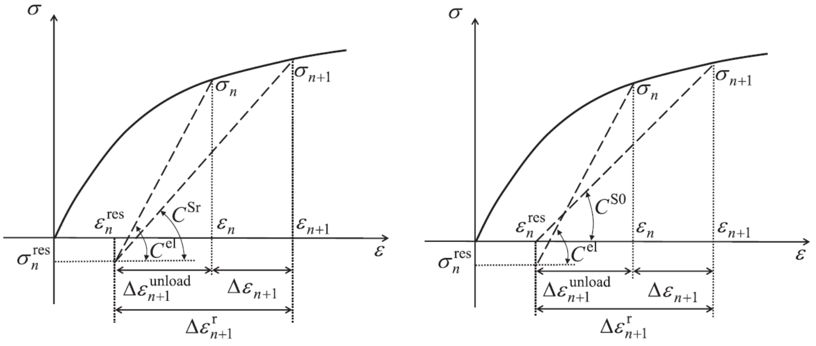

σ
σ_n
σ_{n+1}
$\varepsilon_n^{\mathrm{res}}$
C^{Sr}
C^{el}
ε_n
ε_{n+1}
σ_n^{res}
ε
$\Delta\varepsilon_{n+1}^{\mathrm{unload}}$
$\Delta\varepsilon_{n+1}$
$\Delta\varepsilon_{n+1}^{\mathrm{r}}$
σ
σ_n
σ_{n+1}
C^{S0}
$\varepsilon_n^{\mathrm{res}}$
ε_n
ε_{n+1}
C^{el}
σ_n^{res}
ε
$\Delta\varepsilon_{n+1}^{\mathrm{unload}}$
$\Delta\varepsilon_{n+1}$
$\Delta\varepsilon_{n+1}^{\mathrm{r}}$

(a) Residual–secant (b) Zero–secant

Figure 3.1: Stress strain curves comparing both methods at phase level. (a) Shows the Sr method, or residual-incremental-secant. (b) Shows the S0, or zero-incremental-secant method.

Performing the unloading step consists on solving the system of equations coming from (3.8), the rule of mixtures over the whole composite and the use of the localization tensor in elastic conditions. The latter evaluates the localization tensor at the elastic operator, $\boldsymbol{C}_0^{el}$. The system is thus:

$$\begin{cases} \Delta\bar{\boldsymbol{\varepsilon}}_n^u = v_I \Delta\boldsymbol{\varepsilon}_{I,n}^u + v_0 \Delta\boldsymbol{\varepsilon}_{0,n}^u \\ 0 = v_I \left(\boldsymbol{\sigma}_{I,n} - \boldsymbol{C}_I^{el} : \Delta\boldsymbol{\varepsilon}_{I,n}^u\right) + v_0 \left(\boldsymbol{\sigma}_{0,n} - \boldsymbol{C}_0^{el} : \Delta\boldsymbol{\varepsilon}_{0,n}^u\right) \\ \Delta\boldsymbol{\varepsilon}_{I,n}^u = \boldsymbol{B}\left(\boldsymbol{C}_0^{el}, \boldsymbol{C}_I^{el}\right) : \Delta\boldsymbol{\varepsilon}_{0,n}^u \end{cases} \tag{3.9}$$

The system has been written at time step t_n, but it can also be evaluated at the beginning of the next time step, t_{n+1}. This can depend on the time integration scheme used, or simply on the order in which the algorithm is written (it can be computed at the end of the time step, but remain unused until the next time increment).

Rearranging the system gives the solution as:

$$\begin{cases} \Delta\boldsymbol{\varepsilon}_{0,n}^u = \left(\frac{v_I}{v_0}\boldsymbol{C}_I^{el} : \boldsymbol{B}\left(\boldsymbol{C}_0^{el}, \boldsymbol{C}_I^{el}\right) + \boldsymbol{C}_0^{el}\right)^{-1} : \left(\frac{v_I}{v_0}\boldsymbol{\sigma}_{I,n} + \boldsymbol{\sigma}_{0,n}\right) \\ \Delta\boldsymbol{\varepsilon}_{I,n}^u = \boldsymbol{B}\left(\boldsymbol{C}_0^{el}, \boldsymbol{C}_I^{el}\right) : \Delta\boldsymbol{\varepsilon}_{0,n}^u \\ \Delta\bar{\boldsymbol{\varepsilon}}_n^u = v_I \boldsymbol{B}\left(\boldsymbol{C}_0^{el}, \boldsymbol{C}_I^{el}\right) : \Delta\boldsymbol{\varepsilon}_{0,n}^u + v_0 \Delta\boldsymbol{\varepsilon}_{0,n}^u \end{cases} \tag{3.10}$$

Once the unloading step has been performed, even if the overall residual stress of the composite is zero, this does not happen at phase level. The residual stress that appears at phase level may or may not be considered. This is what defines two different methods. On one hand, the residual-incremental-secant method (abbreviated to "Sr"), which considers the residual stress per phase. On the other hand, the zero-incremental-secant method (S0) considers the residual stress per phase as 0. The difference between each method can also be seen in Figure 3.1.

On the left (3.1 (a)), the operator $\boldsymbol{C}^{Sr}$ allows to reach the stress at the next time step directly from the residual stress. On the right (3.1 (b)), the slope defined by the operator $\boldsymbol{C}^{S0}$ is drawn instead from the point of no residual stress. In both cases, the operator relates the unloaded state with the loaded state at t_{n+1}. The strain increment between these two states is indicated by $\Delta\boldsymbol{\varepsilon}^r_{n+1}$. It is called residual strain increment to indicate that it comes from the residual stress (or unloaded) state.

This $\Delta\boldsymbol{\varepsilon}^r_{n+1}$ is a useful quantity when performing the resolution scheme that allows to define the Linear Comparison Composite in the MFH method. Since the unloading strain $\Delta\boldsymbol{\varepsilon}^u_{r,n+1}$ is a virtual quantity, it can take any sign. Following the convention of the reference paper's work, which is explicited in Figure 3.1, the unloading strain is defined as:

$$\Delta\boldsymbol{\varepsilon}^r_{n+1} = \Delta\boldsymbol{\varepsilon}_{n+1} + \Delta\boldsymbol{\varepsilon}^u_n \tag{3.11}$$

In order to start the MFH computations, an FEM solution is needed for the first step. In this case, the value for the composite strain variation, $\Delta\bar{\boldsymbol{\varepsilon}}^r_{n+1}$ is known from this FEM solution and it is used as input. This is used to have an initial guess on the Inclusion phase strain increment, $\Delta\boldsymbol{\varepsilon}^r_{I,n+1}$, which is set to be equal to the known value $\Delta\bar{\boldsymbol{\varepsilon}}^r_{n+1}$. This guess is used for an iterative procedure, detailed later.

Imposing Equation (3.8) on the composite results in the phases having non-zero residual stresses. These, as well as the residual strains, can be computed through:

$$\begin{cases} \boldsymbol{\sigma}^{res}_{I,n} = \boldsymbol{\sigma}_{I,n} - \boldsymbol{C}^{el}_{I,n} : \Delta\boldsymbol{\varepsilon}^u_{I,n} \\ \boldsymbol{\sigma}^{res}_{0,n} = \boldsymbol{\sigma}_{0,n} - \boldsymbol{C}^{el}_{0,n} : \Delta\boldsymbol{\varepsilon}^u_{0,n} \end{cases} \tag{3.12}$$

$$\begin{cases} \bar{\boldsymbol{\varepsilon}}^{res}_n = \bar{\boldsymbol{\varepsilon}}_n - \Delta\bar{\boldsymbol{\varepsilon}}^u_n \\ \boldsymbol{\varepsilon}^{res}_{I,n} = \boldsymbol{\varepsilon}_{I,n} - \Delta\boldsymbol{\varepsilon}^u_{I,n} \\ \boldsymbol{\varepsilon}^{res}_{0,n} = \boldsymbol{\varepsilon}_{0,n} - \Delta\boldsymbol{\varepsilon}^u_{0,n} \end{cases} \tag{3.13}$$

With the two definitions of operators, the reference paper develops the following definitions of LCC to update the stress at each phase:

$$\begin{cases} \boldsymbol{\sigma}_{r,n+1} = \boldsymbol{\sigma}^{res}_{r,n} + \boldsymbol{C}^{Sr}_r : \Delta\boldsymbol{\varepsilon}^r_{r,n+1} \\ \boldsymbol{\sigma}_{r,n+1} = \boldsymbol{C}^{S0}_r : \Delta\boldsymbol{\varepsilon}^r_{r,n+1} \end{cases} \tag{3.14}$$

The fact that a method uses the residual stresses while the other one sets them to zero produces differences in the stiffness of the results. In the reference paper (by *Wu et al.* [1]) studied the effect of using different combinations of these operators on the two material phases.

Generally, the zero-secant method produces softer results, which are closer to the reality with the use of a first-order method such as this one. The residual-incremental presents over-stiff predictions that are normally paired with second-order methods to become more accurate.

A different version of the radial return mapping has to be used for each operator due to their different considerations of the residual stress. While $\boldsymbol{C}_r^{S0}$ goes with the classical formulation stated in Section 3.3, $\boldsymbol{C}_r^{Sr}$ makes use of the modified formulas. The modification is applied so that the secant operators always remain isotropic. One can define the operators as:

$$\boldsymbol{C}_r^S = 3\kappa^{el}\boldsymbol{I}^{vol} + 2\mu_r^S\boldsymbol{I}^{dev} \tag{3.15}$$

Holding for both cases. Here, κ^{el} is the elastic bulk modulus and μ_r^S is the shear stiffness. A definition of the latter is also provided by the J_2 plasticity model. The expression is taken from *Wu et al.* [1]. For the case in which the residual stresses are not being considered, one has:

$$\mu_r^{S0} = \mu^{el} - \frac{3\left(\mu^{el}\right)^2 \Delta p_{r,n+1}}{\left(\boldsymbol{\sigma}_{r,n+1}^{tr}\right)^{eq}} \tag{3.16}$$

On the other hand, when the residual stresses are being taken into account:

$$\mu_r^{Sr} = \mu^{el} - \frac{3\left(\mu^{el}\right)^2 \Delta p_{r,n+1}}{\left(\Delta\boldsymbol{\sigma}_{r,n+1}^{tr}\right)^{eq}} = \mu^{el} - \frac{3\left(\mu^{el}\right)^2 \Delta p_{r,n+1}}{\left(\boldsymbol{C}^{el} : \Delta\boldsymbol{\varepsilon}_{r,n+1}^{r}\right)^{eq}} \tag{3.17}$$

Here, $\left(\Delta\boldsymbol{\sigma}_{r,n+1}^{tr}\right)^{eq} = \left(\boldsymbol{\sigma}_{r,n+1}^{tr} - \boldsymbol{\sigma}_{r,n}^{res}\right)^{eq}$.

It must be noted that Equations (3.16) and (3.17) are being evaluated at a specific time step, due to their dependency on the plasticity. The term μ^{el} is simply the shear stiffness evaluated when there is no plasticity, i.e., when $\Delta p_r = 0$. Being p the accumulated plastic strain, Δp_r is the increment in plasticity from the previous time step to the next one. This means that evaluating μ_r^S at time t_{n+1} (as expressed by the equations above) makes $\Delta p_r = p_{r,n+1} - p_{r,n}$.

The system of equations to be solved can be now re-written with the use of the residual strain increment. Equations (3.1) and (3.6) are thus finally re-written as:

$$\begin{cases} \Delta\bar{\boldsymbol{\varepsilon}}^r = v_0\Delta\boldsymbol{\varepsilon}_0^r + v_I\Delta\boldsymbol{\varepsilon}_I^r \\ \bar{\boldsymbol{\sigma}} = v_0\boldsymbol{\sigma}_0 + v_I\boldsymbol{\sigma}_I \end{cases} \tag{3.18}$$

$$\Delta\boldsymbol{\varepsilon}_I^r = \boldsymbol{B}\left(\boldsymbol{C}_0^S, \boldsymbol{C}_I^S\right) : \Delta\boldsymbol{\varepsilon}_0^r \tag{3.19}$$

$$\boldsymbol{B}\left(\boldsymbol{C}_0^S, \boldsymbol{C}_I^S\right) = \left\{\boldsymbol{I} + \boldsymbol{S}(\boldsymbol{C}_0^S) : \left[\left(\boldsymbol{C}_0^S\right)^{-1} : \boldsymbol{C}_I^S - \boldsymbol{I}\right]\right\}^{-1} \tag{3.20}$$

Once the operators for each phase are obtained and the stress at the following time step can be calculated, the total macroscopic strain is calculated as:

$$\bar{\boldsymbol{\sigma}}_{n+1} = v_0 \boldsymbol{\sigma}_{0,n+1} + v_I \boldsymbol{\sigma}_{I,n+1} \tag{3.21}$$

Therefore having obtained the updated mechanical state from the stress-train curve. This stress is used for the macroscopic level FEM boundary value problem. Once this one is also converged, the following mechanical states can be calculated in the same fashion.

3.4 MFH as a material law

Here, the procedure followed in [1] to solve the problem is briefly explained. As a remark, the time t_n is sometimes referred to as "previous", whereas "current" is used for t_{n+1}, since it is the one of most interest.

1. The known inputs from the previous time step are:

$$\begin{gathered} \text{Mechanical state: } \bar{\boldsymbol{\varepsilon}}_n, \boldsymbol{\varepsilon}_{r,n}, \bar{\boldsymbol{\sigma}}_n, \boldsymbol{\sigma}_{r,n} \\ \text{Internal variables: } \eta_{r,n} \end{gathered} \tag{3.22}$$

   The internal variables are those that indicate the accumulated plastic strain and strain tensor, as explained in Section 2.1.

   The core function, the constitutive box, is called after second. The following steps are contained inside it.

2. The unloading step explained in Section 3.3 is carried out at the beginning of the time step. This is, unloading from $\boldsymbol{\sigma}_n$ to $\boldsymbol{\sigma}_n^{res}$.

3. Having performed the unloading, one can proceed to solve the MFH. The system of Equations (3.18) to (3.20), which gives the homogenized response, is initialized and solved iteratively.

   The function that calculates the homogenized response is called here. Section 3.5 offers a detailed explanation of the procedure that the function follows to obtain 3.21.

4. The MFH outputs can be retrieved. Namely, the homogenized stress and the jacobian at homogenized level. These have been calculated inside the call to the homogenized response, explained in Section 3.5.

3.5 Homogenization Resolution

This section aims at explaining the resolution of the MFH scheme inside the code. As said, this function is called in steps number 3 and 4 of the function explained in Section 3.4.

1. The first guess on the inclusions strain is initialized inside this function. As explained in Section 3.3, $\Delta\bar{\boldsymbol{\varepsilon}}^r_{n+1}$ is recovered from the FEM solution at this mechanical state. Then, $\Delta\boldsymbol{\varepsilon}^r_{I,n+1}$ is set to be equal to that value. The incremental strain in the matrix phase can then be obtained as $\Delta\boldsymbol{\varepsilon}^r_{0,n+1} = \Delta\bar{\boldsymbol{\varepsilon}}^r_{n+1}$.
2. A Newton-Raphson function is called. Its aim is to iteratively solve the system composed by Equations (3.18) to (3.20), as a function of $\Delta\boldsymbol{\varepsilon}^r_{I,n+1}$. This system is re-written under the form of a residual stress vector, F. This vector can be seen in Equation (3.23).

$$\boldsymbol{F} = \boldsymbol{C}^S_{0,n+1} : \left[\Delta\boldsymbol{\varepsilon}^r_{I,n+1} - \frac{1}{v_0}\boldsymbol{S} : (\boldsymbol{C}^{LCC}_0)^{-1} : \left(\Delta\boldsymbol{\varepsilon}^r_{I,n+1} - \Delta\bar{\boldsymbol{\varepsilon}}^r_{n+1}\right)\right] - \boldsymbol{C}^S_{I,n+1} : \Delta\boldsymbol{\varepsilon}^r_{I,n+1} \tag{3.23}$$

This vector is evaluated at the guessed $\Delta\boldsymbol{\varepsilon}^r_{I,n+1}$ and progressively corrected until it has approached 0 below a specified threshold (normally 10^{-6} or 10^{-4}, depending on the feasibility of obtaining the level of accuracy needed). In order to correct it, the Jacobian, $\boldsymbol{J}$, is calculated and the guessed strain is updated as:

$$\left(\Delta\boldsymbol{\varepsilon}^r_{I,n+1}\right)^{i+1} = \left(\Delta\boldsymbol{\varepsilon}^r_{I,n+1}\right)^{i} - \boldsymbol{J}^{-1} : \boldsymbol{F} \tag{3.24}$$

Here, ”i+1” and ”i” indicate the present and next iteration steps. If the tolerance is not met, the procedure has to be started all over again.

Once the method has converged, Equation (3.21) is used to obtain the homogenized stress over the RVE.

The iterative procedure is thus as follows:

   (a) The elasto-plastic model, explained in Section 2.1 is solved in the first place. With the known inputs from Equation (3.22) and the residual strains obtained during the virtual unloading in Equations (3.12) and (3.13), one can obtain the updated stress, internal variables and the algorithmic tangent operator at the current time step from $\Delta\boldsymbol{\varepsilon}^r_{I,n+1}$.

   In other words, the outputs from the call to this model are $\boldsymbol{\sigma}_{r,n+1}$, $\eta_{r,n+1}$ and $\boldsymbol{C}^{alg}_r$. Note that all of this is computed only at phase level.

   (b) After solving the elasto-plastic model, both load states, t_n and t_{n+1} are known at phase level. Hence, the secant operators are readily obtainable at this point. This means that $\boldsymbol{C}^S_{r,n+1}$ can be obtained from Equation (3.14) depending on the secant method being used for the considered phase.

   (c) With the known secant operators, the Eshelby tensor $\boldsymbol{S}$ also follows from a straightforward computation. The expression for the components of the Eshelby tensor are given by *Wu et al.* in [31] and indicated in Appendix C.

(d) Everything needed to compute the residual stress vector $\boldsymbol{F}$ is now known. Therefore, Equation (3.23) is evaluated.

(e) Likewise, the Jacobian $\boldsymbol{J}$ is also computed. This expression can be found in Appendix B.

(f) The convergence is evaluated, comparing $\boldsymbol{F} = 0$ under a given tolerance. If the result is converged, the loop is exited and the code proceeds to step 3.

(g) In the case that the method has still not converged, the initial guess on the residual strain increment is corrected with Equation (3.24). The residual strain increment in the matrix phase is also updated to be used in the next iteration, as $\left(\Delta\boldsymbol{\varepsilon}^r_{0,n+1}\right)^{i+1} = \left(\left(\Delta\bar{\boldsymbol{\varepsilon}}^r_{n+1}\right)^{i+1} - v_I \Delta\boldsymbol{\varepsilon}^r_{I,n+1}\right)/v_0$. The loop then starts again from step (a) with the new values.

3. After convergence, the average homogenized stress is computed as:

$$\bar{\boldsymbol{\sigma}}_{n+1} = v_0 \boldsymbol{\sigma}_{0,n+1} + v_I \boldsymbol{\sigma}_{I,n+1} \tag{3.25}$$

With this and the macroscopic strain variation, one can also compute the homogenized algorithmic tangent operator at composite level, which is used to characterize the material. From the development in [1], it can be obtained as:

$$\bar{\boldsymbol{C}}^{alg}_{n+1} = v_I \boldsymbol{C}^{alg}_{I,n+1} : \frac{\partial \boldsymbol{\varepsilon}_I}{\partial \bar{\boldsymbol{\varepsilon}}} + v_0 \boldsymbol{C}^{alg}_{0,n+1} : \frac{\partial \boldsymbol{\varepsilon}_0}{\partial \bar{\boldsymbol{\varepsilon}}} \tag{3.26}$$

The phase algorithmic operators $\boldsymbol{C}^{alg}_{I,n+1}$ and $\boldsymbol{C}^{alg}_{0,n+1}$ can be obtained using Equations (2.32) and (2.40), depending on the method used. The term $\dfrac{\partial \boldsymbol{\varepsilon}_r}{\partial \bar{\boldsymbol{\varepsilon}}}$ is also reported in the paper:

$$\frac{\partial \boldsymbol{\varepsilon}_I}{\partial \bar{\boldsymbol{\varepsilon}}} = -\boldsymbol{J}^{-1} : \frac{\partial \boldsymbol{F}}{\partial \bar{\boldsymbol{\varepsilon}}} \quad ; \quad \frac{\partial \boldsymbol{\varepsilon}_0}{\partial \bar{\boldsymbol{\varepsilon}}} = \frac{1}{v_0}\left(\boldsymbol{I} - v_I \frac{\partial \boldsymbol{\varepsilon}_I}{\partial \bar{\boldsymbol{\varepsilon}}}\right) \qquad , \tag{3.27}$$

with $\dfrac{\partial \boldsymbol{F}}{\partial \bar{\boldsymbol{\varepsilon}}} = \dfrac{1}{v_0} \bar{\boldsymbol{C}}^S_0 : \boldsymbol{S}^{-1}$.

After exiting the loop and having computed the outputs, the code performs a series of updates with the obtained information, in order to have the inputs ready for the following time step.

Chapter 4

Continuous formulation

4.1 Derivation of the new localization tensor

As mentioned in previous sections, one of the main drawbacks of the incremental-secant method is its slow convergence with the strain increment. The method converges with the use of smaller strain increments. This is depicted by Figure 4.1.

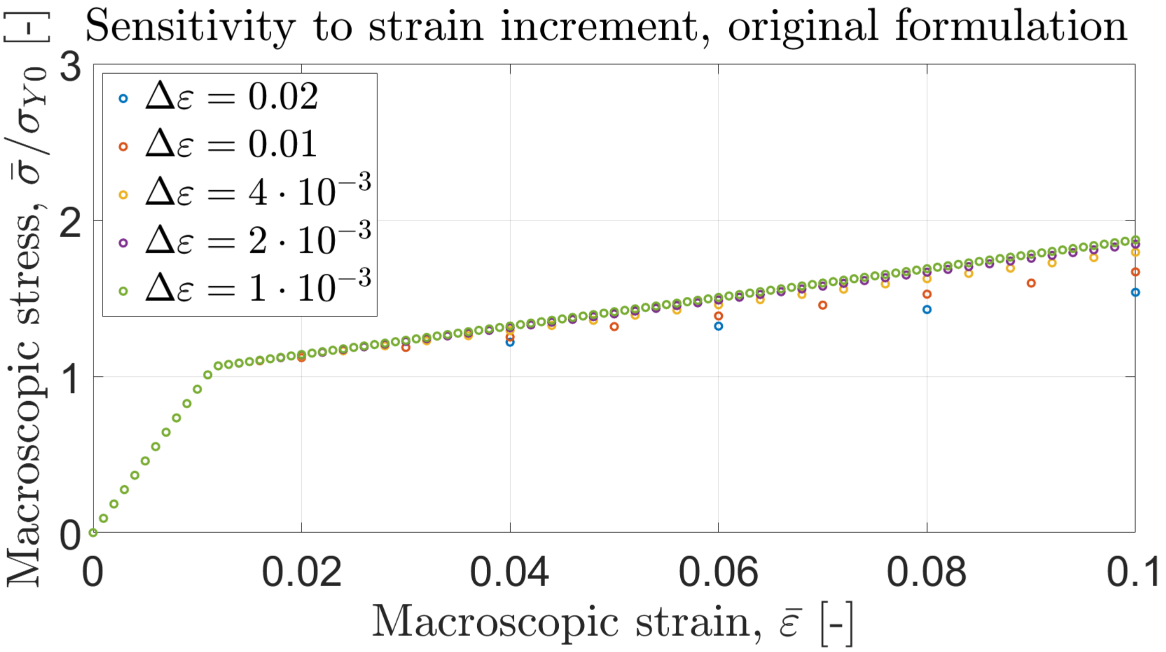

Figure 4.1: Sensitivity to time steps of the incremental-secant formulation.

For a very basic case without strain hardening, whose characteristics are detailed in Tables 4.1 and 4.2, results differ in a visible way as seen in the picture.

Table 4.1: Matrix properties

Matrix properties	
E_0	8.18 GPa
ν_0	0.36
v_0	0.83
σ_{Y0}	100 MPa
$R(p)$	0 MPa

Table 4.2: Inclusion properties

Inclusion properties	
E_I	16.36 GPa
ν_I	0.3636
v_I	0.17
α	1

Therefore, as a means of improving the sensitivity to the time step size, the present work intends to add a variation to the formulation of the strain localization tensor, $\boldsymbol{B}\left(\boldsymbol{C}_0^S, \boldsymbol{C}_I^S\right)$. Note that from now onwards, due to the inclusions being assumed elastic, the strain localization tensor will only have a dependency on the matrix secant operator. It will be therefore written as $\boldsymbol{B}\left(\boldsymbol{C}_0^S, \boldsymbol{C}_I^{el}\right) = \boldsymbol{B}\left(\boldsymbol{C}_0^S\right)$.

This tensor depends on the matrix operator considered and, as such, it can be evaluated at the elastic operator ($\boldsymbol{C}_0^{el}$) or at different definitions of the Linear Comparison Composite operator (LCC). This includes the secant-incremental method or the zero-incremental (as mentioned in Section 3.3).

The new proposed definition for $\boldsymbol{B}\left(\boldsymbol{C}_0^S\right)$ comes from the use of the continuous formulation or, in other words, using an infinitesimal strain increment. This is translated as obtaining an expression for $\boldsymbol{B}\left(\boldsymbol{C}_0^S\right)$ using $d\bar{\boldsymbol{\varepsilon}}$ instead of $\Delta\bar{\boldsymbol{\varepsilon}}$. This is still a first order approximation that takes into consideration small variations around the tensor $\boldsymbol{B}\left(\boldsymbol{C}_0^S\right)$ evaluated at $\boldsymbol{C}_0^{el}$. The expression obtained with this method can afterwards be tested for bigger strain increments.

An important note is that some expressions are derived in the general case and then approximated to the small strain increment. This is equivalent to evaluating some of this expressions at the elastic value. In such cases it is indicated that the expression has been derived in a generic case but being evaluated at this elastic value. This is done by including a vertical bar to the right of the expression. An example for the strain localization tensor is: $\boldsymbol{B}\Big|_{\boldsymbol{C}_0^{el}}$, where the dependency of the function on the secant operator has been made implicit, such that $\boldsymbol{B} = \boldsymbol{B}\left(\boldsymbol{C}_0^S\right)$. Notice that, ultimately, all the expressions whose dependency is evaluated "at the elastic value" are dependent on the shear stiffness, which is the one that is being evaluated at elasticity in the small strain increment limit.

As said, here the strain increment is considered to be infinitesimally small, which allows to consider a series of approximations. First, Equation (3.11) is introduced into (3.19). Then, for the limit case in which the strain increment is very small, one can make $\Delta\bar{\boldsymbol{\varepsilon}}_{n+1} \rightarrow d\bar{\boldsymbol{\varepsilon}}$. This allows to introduce the aforementioned continuous formulation.

Equation (3.11) can be applied to both the macroscopic strain and the strains on the inclusion. This allows re-writting (3.19) as:

$$\left(\boldsymbol{B}(\boldsymbol{C}_0^S)\right)^{-1} : \left(d\boldsymbol{\varepsilon}_I + \Delta\boldsymbol{\varepsilon}_I^u\right) = d\boldsymbol{\varepsilon}_0 + \Delta\boldsymbol{\varepsilon}_0^u \tag{4.1}$$

At the mentioned limit, an approximation can be made, in which the strain localization tensor evaluated at $(\boldsymbol{C}_0^S)$ can be substituted by its evaluation at the elastic operator, plus a small difference coming from its derivative. Rewriting Equation (4.1):

$$\left(\left(\boldsymbol{B}\Big|_{\boldsymbol{C}_0^{el}}\right)^{-1} + \frac{d\left(\boldsymbol{B}(\boldsymbol{C}_0^S)\right)^{-1}}{d\mu_r^S}\Big|_{\boldsymbol{C}_0^{el}} d\mu_r^S\right) : (d\boldsymbol{\varepsilon}_I + \Delta\boldsymbol{\varepsilon}_I^u) = d\boldsymbol{\varepsilon}_0 + \Delta\boldsymbol{\varepsilon}_0^u \tag{4.2}$$

Developing the product results in:

$$\left(\boldsymbol{B}\Big|_{\boldsymbol{C}_0^{el}}\right)^{-1} : d\boldsymbol{\varepsilon}_I + \left(\boldsymbol{B}\Big|_{\boldsymbol{C}_0^{el}}\right)^{-1} : \Delta\boldsymbol{\varepsilon}_I^u + \frac{d\left(\boldsymbol{B}(\boldsymbol{C}_0^S)\right)^{-1}}{d\mu_r^S}\Big|_{\boldsymbol{C}_0^{el}} d\mu_r^S : d\boldsymbol{\varepsilon}_I + \frac{d\left(\boldsymbol{B}(\boldsymbol{C}_0^S)\right)^{-1}}{d\mu_r^S}\Big|_{\boldsymbol{C}_0^{el}} d\mu_r^S : \Delta\boldsymbol{\varepsilon}_I^u = d\boldsymbol{\varepsilon}_0 + \Delta\boldsymbol{\varepsilon}_0^u \tag{4.3}$$

The term $\frac{d\left(\boldsymbol{B}(\boldsymbol{C}_0^S)\right)^{-1}}{d\mu_r^S}\Big|_{\boldsymbol{C}_0^{el}} d\mu_r^S : d\boldsymbol{\varepsilon}_I$ contains a multiplication of two differentials. Since this is a first order approximation, second order terms are neglected, therefore it is disregarded. Furthermore, the term $\left(\boldsymbol{B}\Big|_{\boldsymbol{C}_0^{el}}\right)^{-1} : \Delta\boldsymbol{\varepsilon}_I^u$ is, by definition of the localization tensor, equal to $\Delta\boldsymbol{\varepsilon}_0^u$. The reason behind this is that, as said, for the virtual unloading one always uses the elastic operator. This allows to cancel the unloading strain term in the RHS, eliminating the influence of most of the elastic part of the strain.

The derivative of $\mathbf{B}^{-1}$ can be obtained from its expression in Equation (3.20).

$$\boldsymbol{B}(\boldsymbol{C}_0^S)^{-1} = \boldsymbol{I} + \boldsymbol{S}\left(\boldsymbol{C}^S\right) : \left[\left(\boldsymbol{C}_0^S\right)^{-1} : \boldsymbol{C}_I^S - \boldsymbol{I}\right] = \boldsymbol{I} + \boldsymbol{P} : \left[\boldsymbol{C}_I^S - \boldsymbol{C}_0^S\right]$$

Here, the equivalence with the definition using the Hill tensor $\boldsymbol{P}$ has been shown simply to indicate that this method can be followed with either Eshelby or Hill ([32]) tensors. Each of them presents slightly different characteristics that allow to choose between them as a matter of convenience. They can be related through:

$$\boldsymbol{P} = \boldsymbol{S} : \left(\boldsymbol{C}_0^S\right)^{-1}$$

Back to the derivative of the localization tensor, one has:

$$\frac{d\left(\boldsymbol{B}(\boldsymbol{C}_0^S)\right)^{-1}}{d\mu_0^S} = \frac{d\boldsymbol{S}(\boldsymbol{C}_0^S)}{d\mu_0^S} : \left(\left(\boldsymbol{C}_0^S\right)^{-1} : \boldsymbol{C}_I^S - \boldsymbol{I}\right) + \boldsymbol{S}(\boldsymbol{C}_0^S) : \frac{\partial\left(\boldsymbol{C}_0^S\right)^{-1}}{\partial\mu_0^S} : \boldsymbol{C}_I^S \tag{4.4}$$

In the present case, this expression is evaluated[1] at $\boldsymbol{C}_0^{el}$. Recall that the secant operators are defined as $\boldsymbol{C}^S = 3\kappa^{el} I^{vol} + 2\mu_r^S \boldsymbol{I}^{dev}$, with κ^{el} the elastic bulk modulus, so that the elastic value of the operator is at $\mu_r^S = \mu^{el}$.

---

[1] The expressions are first derivated and then evaluated at the corresponding point. Due to this, the derivative of $\left(\boldsymbol{C}_0^S\right)^{-1}$ with respect to μ_0^S becomes $-2\left(\boldsymbol{C}_0^{el}\right)^{-1} : \boldsymbol{I}^{dev} : \left(\boldsymbol{C}_0^{el}\right)^{-1}$ after being evaluated.

Equation (4.4) can be introduced into (4.3) to obtain:

$$\begin{aligned}\left(\boldsymbol{B}\Big|_{\boldsymbol{C}_0^{el}}\right)^{-1} : d\boldsymbol{\varepsilon}_I = \Bigg\{ I - \Bigg[\frac{d\boldsymbol{S}}{d\mu_0^S}\Big|_{\boldsymbol{C}_0^{el}} : \left(\left(\boldsymbol{C}_0^{el}\right)^{-1} : \boldsymbol{C}_I^S - I\right) - \\ 2\boldsymbol{S}\Big|_{\boldsymbol{C}_0^{el}} : \left(\boldsymbol{C}_0^{el}\right)^{-1} : \boldsymbol{I}^{dev} : \left(\boldsymbol{C}_0^{el}\right)^{-1} : \boldsymbol{C}_I^S\Bigg] : \Delta\boldsymbol{\varepsilon}_I^u \otimes \frac{\partial \mu_0^S}{\partial \boldsymbol{\varepsilon}_0}\Bigg\} : d\boldsymbol{\varepsilon}_0\end{aligned} \tag{4.5}$$

Pre-multiplying by $\boldsymbol{B}\Big|_{\boldsymbol{C}_0^{el}}$ and introducing the temporal variation into the strain differentials yields:

$$\begin{aligned}\dot{\boldsymbol{\varepsilon}}_I = \Bigg\{\boldsymbol{B}\Big|_{\boldsymbol{C}_0^{el}} - \boldsymbol{B}\Big|_{\boldsymbol{C}_0^{el}} : \Bigg[\frac{d\boldsymbol{S}}{d\mu_0^S}\Big|_{\boldsymbol{C}_0^{el}} : \left(\left(\boldsymbol{C}_0^{el}\right)^{-1} : \boldsymbol{C}_I^S - I\right) - \\ 2\boldsymbol{S}\Big|_{\boldsymbol{C}_0^{el}} : \left(\boldsymbol{C}_0^{el}\right)^{-1} : \boldsymbol{I}^{dev} : \left(\boldsymbol{C}_0^{el}\right)^{-1} : \boldsymbol{C}_I^S\Bigg] : \Delta\boldsymbol{\varepsilon}_I^u \otimes \frac{\partial \mu_0^S}{\partial \boldsymbol{\varepsilon}_0}\Bigg\} : \dot{\boldsymbol{\varepsilon}}_0\end{aligned} \tag{4.6}$$

The expression in braces can be grouped into a single matrix called, for example, $\boldsymbol{B}^{Cont}\left(\Delta\boldsymbol{\varepsilon}_I^u, \frac{\partial\mu_0^S}{\partial\boldsymbol{\varepsilon}_0}\right)$. This is the new localization tensor used in the resolution scheme. This new tensor can be written as:

$$\boldsymbol{B}^{Cont} = \boldsymbol{B}\Big|_{\boldsymbol{C}_0^{el}} - \boldsymbol{B}\Big|_{\boldsymbol{C}_0^{el}} : \left[\frac{d\boldsymbol{S}}{d\mu_0^S}\Big|_{\boldsymbol{C}_0^{el}} : \left(\left(\boldsymbol{C}_0^{el}\right)^{-1} : \boldsymbol{C}_I^S - I\right) - 2\boldsymbol{S}\Big|_{\boldsymbol{C}_0^{el}} : \left(\boldsymbol{C}_0^{el}\right)^{-1} : \boldsymbol{I}^{dev} : \left(\boldsymbol{C}_0^{el}\right)^{-1} : \boldsymbol{C}_I^S\right] : \Delta\boldsymbol{\varepsilon}_I^u \otimes \frac{\partial\tilde{\mu}_0^S}{\partial\boldsymbol{\varepsilon}_0} \tag{4.7}$$

The derivative of the Eshelby tensor, $\dfrac{d\boldsymbol{S}}{d\mu_0^S}$ is developed in Appendix C.

Notice the addition of the tilde over the derivative of the shear stiffness in Equation (4.7). This is once more a result of making the approximation of the continuous formulation, in which the time step approaches zero and thus the functions of the shear stiffness approach their elastic value.

To obtain this term, one starts at Equation (3.16):

$$\mu^{S0} = \mu^{el} - \frac{3(\mu^{el})^2\Delta p}{(\boldsymbol{\sigma}^{tr})^{eq}} \tag{4.8}$$

One can express the derivative of μ^{S0} as:

$$\frac{\partial\mu^{S0}}{\partial\boldsymbol{\varepsilon}} = \frac{1}{(\boldsymbol{\sigma}^{tr})^{eq}}\left[\mu^{el}\frac{\partial\left(\boldsymbol{\sigma}^{tr}\right)^{eq}}{\partial\boldsymbol{\varepsilon}} - 3\left(\mu^{el}\right)^2\frac{\partial\Delta p}{\partial\boldsymbol{\varepsilon}} - \mu^{S0}\frac{\partial\left(\boldsymbol{\sigma}^{tr}\right)^{eq}}{\partial\boldsymbol{\varepsilon}}\right] \tag{4.9}$$

In order to develop this equation, one has to use the derivatives developed in Section (2.4). More specifically, Equations (2.28) and (2.29) can be plugged in:

$$\frac{\partial\mu^{S0}}{\partial\boldsymbol{\varepsilon}} = \frac{2\mu^{el}}{(\boldsymbol{\sigma}^{tr})^{eq}}\left[\mu^{el} - \frac{3\left(\mu^{el}\right)^2}{h} - \mu^{S0}\right]\boldsymbol{N} \tag{4.10}$$

Introducing the equation of μ^{S0} and rearranging gives a more simplified final expression:

$$\frac{\partial \mu^{S0}}{\partial \boldsymbol{\varepsilon}} = \frac{6\left(\mu^{el}\right)^3}{\left(\boldsymbol{\sigma}^{tr}\right)^{eq}} \left[\frac{\Delta p}{\left(\boldsymbol{\sigma}^{tr}\right)^{eq}} - \frac{1}{h}\right] \boldsymbol{N} \tag{4.11}$$

It is important to comment that the continuous strain localization operator uses its formulas in the approach to elastic values, this is, for very small strain increments. This is the reason why, for example, the Eshelby tensors used in Equation (4.7) are evaluated at the elastic shear stiffness. In the same fashion, (4.11) can be adapted to this limit by setting $\Delta p = 0$ and yielding a simpler equation.

$$\frac{\partial \tilde{\mu}^{S0}}{\partial \boldsymbol{\varepsilon}} = \frac{-6\left(\mu^{el}\right)^3}{\left(\boldsymbol{\sigma}^{tr}\right)^{eq} h} \boldsymbol{N} \tag{4.12}$$

Equation (4.12) is the one to be used for the subsequent evaluations of the derivative of μ^{S0}. On the other hand, for μ^{Sr}, one begins with Equation (3.17):

$$\mu^{Sr} = \mu^{el} - \frac{3(\mu^{el})^2 \Delta p}{\left(\Delta\boldsymbol{\sigma}^{tr}\right)^{eq}} = \mu^{el} - \frac{3(\mu^{el})^2 \Delta p}{\left(\boldsymbol{C}^{el} : \Delta\boldsymbol{\varepsilon}^{r}\right)^{eq}} \tag{4.13}$$

The procedure to obtain the derivative is similar as with the zero-incremental method.

$$\frac{\partial \mu^{Sr}}{\partial \boldsymbol{\varepsilon}} = \frac{1}{\left(\Delta\boldsymbol{\sigma}^{tr}\right)^{eq}} \left[\mu^{el} \frac{\partial \left(\Delta\boldsymbol{\sigma}^{tr}\right)^{eq}}{\partial \boldsymbol{\varepsilon}} - 3\left(\mu^{el}\right)^2 \frac{\partial \Delta p}{\partial \boldsymbol{\varepsilon}} - \mu^{Sr} \frac{\partial \left(\Delta\boldsymbol{\sigma}^{tr}\right)^{eq}}{\partial \boldsymbol{\varepsilon}}\right] \tag{4.14}$$

The term $\dfrac{\partial \left(\Delta\boldsymbol{\sigma}^{tr}\right)^{eq}}{\partial \boldsymbol{\varepsilon}}$ is:

$$\frac{\partial \left(\Delta\boldsymbol{\sigma}^{tr}\right)^{eq}}{\partial \boldsymbol{\varepsilon}} = 2\mu^{el} \boldsymbol{N}_m \tag{4.15}$$

Recovering the term $\dfrac{\partial \Delta p}{\partial \boldsymbol{\varepsilon}}$ from Equation (2.38) and setting $\Delta p = 0$ allows to write:

$$\frac{\partial \tilde{\mu}^{Sr}}{\partial \boldsymbol{\varepsilon}} = \frac{-6\left(\mu^{el}\right)^3}{\left(\Delta\boldsymbol{\sigma}^{tr}\right)^{eq} h_m} \boldsymbol{N} \tag{4.16}$$

This is the expression to be used when evaluating the derivative of the residual-incremental shear stiffness, μ_0^{Sr}.

The expression for this new strain localization tensor can be evaluated at different times, depending on the numerical scheme used for the integration of Equation (4.6). This varies the points at which

$\frac{\partial \tilde{\mu}_0^S}{\partial \boldsymbol{\varepsilon}_0}$ is considered. Likewise, $\Delta \boldsymbol{\varepsilon}_I^u$ can be evaluated at either t_n or t_{n+1}, although its value is expected to change less.

Explicit schemes, such as the forward Euler, will evaluate both of these functions at the previous time steps, i.e., t_n when one wants to compute the macroscopic mechanical state at t_{n+1}. Implicit schemes will either only use their evaluation at t_{n+1} (backward Euler) or use a mix of both (Crank-Nicholson scheme). In the present work, the implicit backward Euler is the scheme used.

4.2 MFH system

A priori, the major advantage of using a continuous formulation is allowing a bigger strain increment to be used while keeping a good accuracy, once a discretization is chosen. This is still intended to be used under the frame of the incremental-secant method.

The main difference of the CS formulation is that, with the aim of having a better approach at the continuous nature of the materials, the strain localization tensor $\boldsymbol{B}^{Cont}$ is derived before introducing the finite differences in the method. This can be appreciated by the substitution of the differentials $d\boldsymbol{\varepsilon}$ by the finite strain increments $\Delta\boldsymbol{\varepsilon}$ between Equations (4.6) and (4.18).

In this work, the input used is not the residual strain increment, but rather the strain increment from t_n to t_{n+1}, both at loaded state. Therefore, the system of equations that is intended to solve is still the same as in Section 3.3. Equations (3.18) and (3.19) are re-written as:

$$\begin{cases} \Delta\bar{\boldsymbol{\varepsilon}} = v_0 \Delta\boldsymbol{\varepsilon}_0 + v_I \Delta\boldsymbol{\varepsilon}_I \\ \bar{\boldsymbol{\sigma}} = v_0 \boldsymbol{\sigma}_0 + v_I \boldsymbol{\sigma}_I \end{cases} \tag{4.17}$$

$$\Delta\boldsymbol{\varepsilon}_I = \boldsymbol{B}^{Cont} : \Delta\boldsymbol{\varepsilon}_0 \tag{4.18}$$

Lastly, Equation (3.20) is updated to the new definition of the strain localization tensor given by Equation (4.7).

The resolution of this new system of equations is performed by adding modifications to the code used in the reference paper. The resolution scheme is detailed in the next section and follows a similar structure.

Note that here the continuous formulation has already been discretized. One can do this with any time discretization in order to apply different integration methods to the same model definition. Given that the continuous strain localization tensor depends mainly on the unloading strain of the inclusion and on the shear stiffness derivative of the matrix, the type of discretization (implicit, explicit, etc...) is given by the choice of these two variables.

The work has been performed by using an implicit time scheme to compute the new tensor. The term $\dfrac{\partial \tilde{\mu}_r^S}{\partial \boldsymbol{\varepsilon}_0}$ is evaluated at t_{n+1} (therefore being an implicit term). However, $\Delta\boldsymbol{\varepsilon}_I^u$ is evaluated simply at t_n, although its evaluation time could also be set to either t_{n+1} or a mid-point. The basis for the validity of this is that the unloading strain varies only slightly between the different mechanical states. The shear stiffness derivative, on the other hand, presents greater variations and thus must be evaluated implicitly.

From now onwards, this method will be referred to as Continuous-Secant (CS) discretization. This is not to give an official name, but rather to make a simple distinction with respect to the original in chapters where several references to both have to be made.

4.3 Constitutive box

In this section the resolution scheme is explained thoroughly. As said, it is based mainly on the work presented in Section 3.3.

1. The internal variables, strains and stresses at the previous time step are known. Again:

$$\begin{gathered}\text{Mechanical state: } \bar{\boldsymbol{\varepsilon}}_n, \boldsymbol{\varepsilon}_{r,n}, \bar{\boldsymbol{\sigma}}_n, \boldsymbol{\sigma}_{r,n}\\ \text{Internal variables: } \eta_{r,n}\end{gathered} \tag{4.19}$$

2. The virtual elastic unloading is performed at the previous time step. $\boldsymbol{\sigma}_n^{res}$ and $\boldsymbol{\varepsilon}_n^{res}$ are thus obtained at phases and at composite level. Note that now the unloading strain at inclusions phase, $\Delta\boldsymbol{\varepsilon}_I^u$ is kept as an important value, since it is needed to later compute $\boldsymbol{B}^{Cont}$.

   Due to the strain localization tensor being evaluated with the elastic operator, the unloading can be done at this point. As mentioned in Chapter 3, the unloading system is defined in Equation (3.9). The solution presented in terms of $\boldsymbol{B}$ can be recovered and adapted to the slight differences in notation:

$$\begin{cases}\Delta\boldsymbol{\varepsilon}_{0,n}^u = \left(\frac{v_I}{v_0}\boldsymbol{C}_I^{el} : \boldsymbol{B}\Big|_{\boldsymbol{C}_0^{el}} + \boldsymbol{C}_0^{el}\right)^{-1} : \left(\frac{v_I}{v_0}\boldsymbol{\sigma}_{I,n} + \boldsymbol{\sigma}_{0,n}\right)\\ \Delta\boldsymbol{\varepsilon}_{I,n}^u = \boldsymbol{B}\Big|_{\boldsymbol{C}_0^{el}} : \Delta\boldsymbol{\varepsilon}_{0,n}^u\\ \Delta\bar{\boldsymbol{\varepsilon}}_n^u = v_I\boldsymbol{B}\Big|_{\boldsymbol{C}_0^{el}} : \Delta\boldsymbol{\varepsilon}_{0,n}^u + v_0\Delta\boldsymbol{\varepsilon}_{0,n}^u\end{cases} \tag{4.20}$$

   Equations (3.12) and (3.13) do not present any change and are used as they are in this method.

3. The function that solves the MFH system is called at this step. Like done previously, this function is explained in-depth separately, in Section 4.4.

4. The outputs obtained in the MFH function are retrieved here as a result of the time step. These are used as inputs into the macroscopic-level solver. This solver computes a suitable equilibrium equation resolution with the given $\bar{\boldsymbol{\sigma}}$.

4.4 Homogenization resolution

The function that solves the MFH system, this time posed by Equations (4.17) and (4.18), along with B^{cont} from Equation (4.7). The process is the following:

1. In this case, the scheme starts by giving an initial guess to $\Delta\boldsymbol{\varepsilon}_{I,n+1}$. As mentioned before, this guess is drawn from the FEM solution, since the resulting macro-scale strain is considered given. Therefore, the first value is initialized as: $\Delta\boldsymbol{\varepsilon}_{I,n+1} = \Delta\bar{\boldsymbol{\varepsilon}}_{n+1}$ [2].

   The strains in the matrix are also initialized as $\Delta\boldsymbol{\varepsilon}_{0,n+1} = \Delta\bar{\boldsymbol{\varepsilon}}_{n+1}$.

2. The Newton-Raphson loop can be entered. Again, the resolution method is based on using a residual function $\boldsymbol{F}$ that is iteratively compared to 0. In this case, the variable to be corrected in each iteration is the strain increment between steps in the inclusions phase: $\Delta\boldsymbol{\varepsilon}_{I,n+1}$.

   Equation (4.17) is re-written under the form of this residual function as:

   $$\boldsymbol{F} = v_0 \left(\boldsymbol{B}_{n+1}^{Cont}\right)^{-1} : \Delta\boldsymbol{\varepsilon}_{I,n+1} + v_I \Delta\boldsymbol{\varepsilon}_{I,n+1} - \Delta\bar{\boldsymbol{\varepsilon}}_{n+1} \tag{4.21}$$

   Where $\boldsymbol{B}_{n+1}^{Cont} = \boldsymbol{B}^{Cont}\left(\Delta\boldsymbol{\varepsilon}_{I,n}^{u}, \dfrac{\partial\tilde{\mu}_{0,n+1}^{S}}{\partial\boldsymbol{\varepsilon}_0}\right)$ and the strain increments can be calculated from last step as $\Delta\boldsymbol{\varepsilon}_{n+1} = \boldsymbol{\varepsilon}_{n+1} - \boldsymbol{\varepsilon}_n$.

   To obtain the localization tensor, it is necessary to previously evaluate $\dfrac{\partial\tilde{\mu}_{0,n+1}^{S}}{\partial\boldsymbol{\varepsilon}_0}$ at the current time step. Recall that the approximation to small time steps used, so that $\dfrac{\partial\tilde{\mu}_{0,n+1}^{S}}{\partial\boldsymbol{\varepsilon}_0}$ is in fact used in the code. This term is obtained in Appendix D. Depending on the method used, either Equation (4.22) or (4.23) has to be used.

   $$\frac{\partial\tilde{\mu}^{Sr}}{\partial\boldsymbol{\varepsilon}} = \frac{-6\left(\mu^{el}\right)^3}{\left(\Delta\boldsymbol{\sigma}^{tr}\right)^{eq} h_m}\boldsymbol{N} \tag{4.22}$$

   $$\frac{\partial\tilde{\mu}^{S0}}{\partial\boldsymbol{\varepsilon}} = \frac{-6\left(\mu^{el}\right)^3}{\left(\boldsymbol{\sigma}^{tr}\right)^{eq} h}\boldsymbol{N} \tag{4.23}$$

   The increment in the inclusions phase is corrected as

   $$\left(\Delta\boldsymbol{\varepsilon}_{I,n+1}\right)^{i+1} = \left(\Delta\boldsymbol{\varepsilon}_{I,n+1}\right)^{i} - \boldsymbol{J}^{-1} : \boldsymbol{F} \qquad , \tag{4.24}$$

   being the expression for $\boldsymbol{J}$ provided in Appendix E, as it has a different expression from the one used in Section 3.5.

   The iterative procedure is:

---

[2] This particular assumption corresponds to the so-called Voigt assumption for axial loading. Roughly, it means assuming that the strains are evenly distributed over the two phases. The application of both this and the Reuss estimate are detailed in by *Hill* in [33].

(a) The elasto-plastic model can be solved in the first place with the information known at this point.

(b) The residual increment of strain $\Delta\boldsymbol{\varepsilon}^r_{n+1}$, needed to evaluate $\Delta\sigma^r_{n+1}$, can be obtained as:

$$\Delta\boldsymbol{\varepsilon}^r_{n+1} = \Delta\boldsymbol{\varepsilon}_{n+1} + \Delta\boldsymbol{\varepsilon}^u_n \qquad , \tag{4.25}$$

for both phases. Then, the shear stiffness is computed with the corresponding equation depending on the method. Their derivatives are also evaluated at this point, again with Equation (4.22) or (4.23).

(c) The Eshelby tensor is computed afterwards. Its expression is still the one given in Appendix C.

(d) Everything is needed to evaluate the residual function $\boldsymbol{F}$ from Equation (4.21).

(e) The Jacobian $\boldsymbol{J}$ is also evaluated, see Appendix E.

(f) Again, the convergence is assessed within the user-specified tolerances. If the solution is accurate enough, the loop is exited and the outputs are calculated. If it is not, the next step is conducted to correct the guess on the strains.

Furthermore, the residual is also compared to the one from the previous iteration. This is done in order to ensure that the residuals keep decreasing each time, so that the iterative process is actually converging towards a solution. The correction applied to the strain is reduced in case that the residual has increased; and the loop is exited with an error if the corrections are not useful to make the procedure converge.

(g) The correction in Equation (4.27) is applied to obtain a value for $(\Delta\boldsymbol{\varepsilon}_{I,n+1})^{i+1}$. The strain in the matrix is also re-computed with the new value of the inclusion strain with the formula:

$$\Delta\boldsymbol{\varepsilon}_{0,n+1} = (\Delta\bar{\boldsymbol{\varepsilon}}_{n+1} - v_I\Delta\boldsymbol{\varepsilon}_{I,n+1})/v_0 \tag{4.26}$$

3. After convergence, outputs are obtained. Recovering the equations from the incremental-secant method, one has:

$$\bar{\boldsymbol{\sigma}}_{n+1} = v_0\boldsymbol{\sigma}_{0,n+1} + v_I\boldsymbol{\sigma}_{I,n+1} \tag{4.27}$$

For the macroscopic algorithmic operator,

$$\bar{\boldsymbol{C}}^{alg}_{n+1} = v_I\boldsymbol{C}^{alg}_{I,n+1} : \frac{\partial\boldsymbol{\varepsilon}_I}{\partial\bar{\boldsymbol{\varepsilon}}} + v_0\boldsymbol{C}^{alg}_{0,n+1} : \frac{\partial\boldsymbol{\varepsilon}_0}{\partial\bar{\boldsymbol{\varepsilon}}} \qquad , \tag{4.28}$$

The phase algorithmic operators can be obtained by the use of Equations (2.32) or (2.40), depending on the method.

Finally:

$$\frac{\partial\boldsymbol{\varepsilon}_I}{\partial\bar{\boldsymbol{\varepsilon}}} = -\boldsymbol{J}^{-1} : \frac{\partial\boldsymbol{F}}{\partial\bar{\boldsymbol{\varepsilon}}} \quad ; \quad \frac{\partial\boldsymbol{\varepsilon}_0}{\partial\bar{\boldsymbol{\varepsilon}}} = \frac{1}{v_0}\left(\boldsymbol{I} - v_I\frac{\partial\boldsymbol{\varepsilon}_I}{\partial\bar{\boldsymbol{\varepsilon}}}\right) \qquad , \tag{4.29}$$

with $\dfrac{\partial\boldsymbol{F}}{\partial\bar{\boldsymbol{\varepsilon}}} = -\boldsymbol{I}$.

Chapter 5

Analysis of the results

As it was mentioned in the beginning, the objective of this work is to prove if the approach of the continuous formulation is indeed a useful modification of the residual-incremental formulation developed by *Wu et al.* in [1]. Therefore, the first section of this chapter is devoted to analyzing the reliability of the implemented code by comparing the CS discretization with the results of the original code developed in [1]. This is first done via a test with simple conditions. Once the reliability of the formulation is proved, its reduced sensitivity to strain increments is demonstrated. Latter sections showcase the adaptability of the CS discretization method to more complex computations. The material properties of each case are also drawn from [1] and used as a basis for comparison. Lastly, the results used in that paper to serve as basis are used here for comparison. These results come from methods such as direct finite element simulations (FE), Fast Fourier Transforms or experimental results.

The main points of interest of the method developed here can be recalled now. Firstly, having a continuous formulation allows for the use of any time discretization scheme that one wants. Secondly, given how this formulation is defined, for an infinitely small strain increment, its results should converge to the ones of the original formulation. Lastly, the discretizations achieved should be less sensitive to an increase in strain increment size (when comparing models of the same order between the original formulation and the new one).

Unless stated otherwise, the results shown here correspond to uni-axial tests.

5.1 Reliability of the approach

5.1.1 Convergence with strain increments

The first step to be able to test the code and compare it, is to check that, in fact, the code has achieved convergence with the strain increments. As user input, an increasing number of strain increments was used (so, $\Delta\varepsilon$ becomes smaller) in order to see when this stopped affecting the results.

For simplicity, the modification of the base code is tested first in a case of uniaxial tension and no strain hardening. The conditions are:

Table 5.1: Matrix properties

Matrix properties	
E_0	75 GPa
ν_0	0.3
v_0	0.85
σ_{Y0}	75 MPa
$R(p)$	0 MPa

Table 5.2: Inclusion properties

Inclusion properties	
E_I	400 GPa
ν_I	0.2
v_I	0.15
α	1

Furthermore, inclusions are considered elastic and are spherical with the given aspect ratio $\alpha = 1$.

The size of strain increments for the different computations is: $\Delta\varepsilon = 1 \cdot 10^{-3}$; $2 \cdot 10^{-5}$; and $4 \cdot 10^{-6}$. The stress-strain curve of the composite (i.e., the macroscopic curve) under uniaxial loading is plotted for each one of these strain increment sizes. Figure 5.1 shows the results for the convergence of the CS discretization using both residual (use of Equation (4.22)) and zero residual stresses (employing Equation (4.23)), as well as the results using the original code with $\boldsymbol{C}^{Sr}$ and $\boldsymbol{C}^{S0}$.

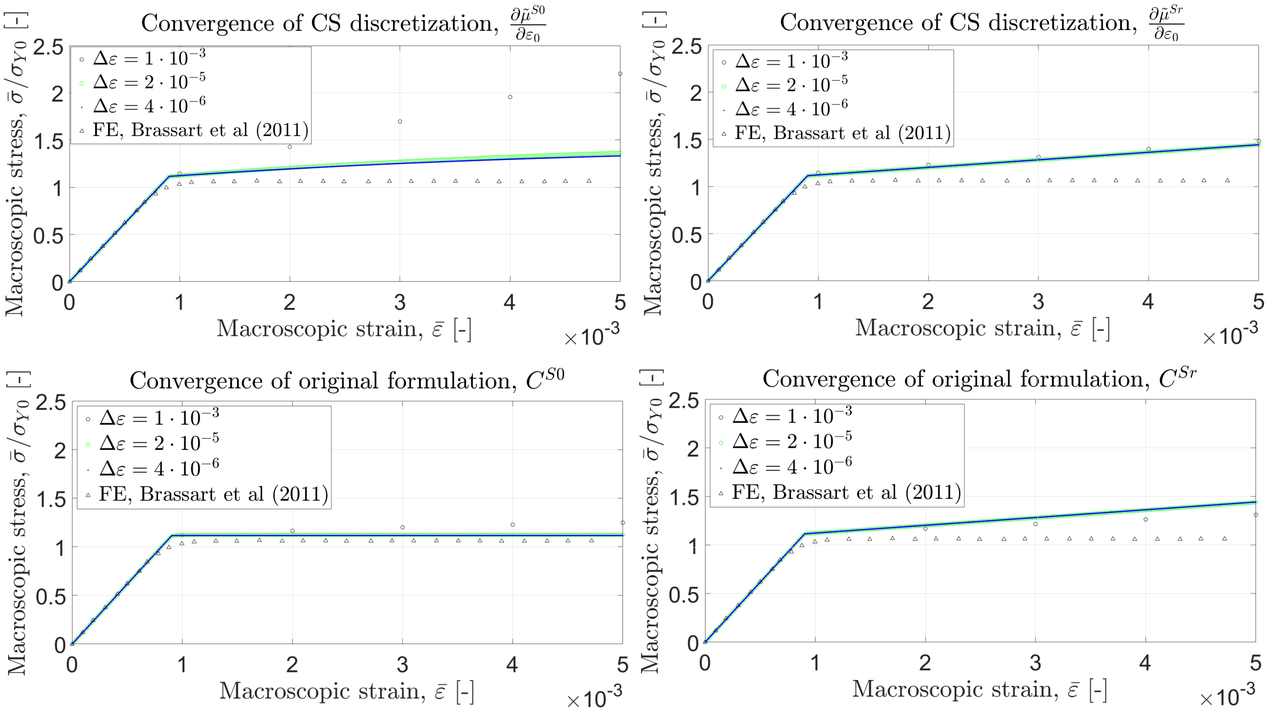

Figure 5.1: Convergence of the CS discretization using C^{Sr}. FE results from *Brassart et al.* [6]

For both cases, C^{Sr} and C^{S0}, the lines converge from, at least, $\Delta\varepsilon = 2 \cdot 10^{-5}$ onwards. The residual case seems to be presenting convergence much before, since the three lines are very close together. The zero method, however, needs a bigger reduction of the strain increment. In any case the lines appear to indicate a convergence of the results. The macroscopic stress can be set as a figure of merit to measure the accuracy of the calculations.

More precisely, its value at the last converged strain increment is the one used. The reason behind this is that, since the elastic region is linear, any strain increment used gives the exact same solutions. Therefore the difference in results starts at the yielding point and grows with computations. Looking the converged value at the last strain increment indicates the maximum shift between two different $\Delta\varepsilon$ curves.

Tables 5.3 through 5.6 showcase the values of $\bar{\sigma}$ for each of the strain increments tested. Furthermore, the relative error column shows the variation of results with respect to $\Delta\varepsilon = 4 \cdot 10^{-6}$.

Table 5.3: Residual-incremental accuracy of CS discretization.

CS discretization: Residual-incremental		
$\Delta\varepsilon$ [-]	$\bar{\sigma}$ [MPa]	Relative error
$4 \cdot 10^{-6}$	190.257	0%
$2 \cdot 10^{-5}$	190.234	0.012%
$1 \cdot 10^{-3}$	189.664	0.412%

Table 5.4: Residual-incremental accuracy of original formulation.

Original formulation: Residual-incremental		
$\Delta\varepsilon$ [-]	$\bar{\sigma}$ [MPa]	Relative error
$4 \cdot 10^{-6}$	190.247	0%
$2 \cdot 10^{-5}$	190.228	0.009%
$1 \cdot 10^{-3}$	1.526%	1.526%

Table 5.5: Zero-incremental accuracy of CS discretization.

CS discretization: Zero-incremental		
$\Delta\varepsilon$ [-]	$\bar{\sigma}$ [MPa]	Relative error
$4 \cdot 10^{-6}$	156.334	0%
$2 \cdot 10^{-5}$	156.662	-0.210%
$1 \cdot 10^{-3}$	174.937	-11.900%

Table 5.6: Zero-incremental accuracy of original formulation.

Original formulation: Zero-incremental		
$\Delta\varepsilon$ [-]	$\bar{\sigma}$ [MPa]	Relative error
$4 \cdot 10^{-6}$	106.364	0%
$2 \cdot 10^{-5}$	106.484	-0.113%
$1 \cdot 10^{-3}$	112.954	-6.196%

In the residual-incremental case, there is a clear improvement of the error coming from the use of the CS discretization. The relative error drops from 1.526% to only 0.412%. In the zero-incremental case, it looks like the original formulation is still better. This is due to the CS discretization results becoming stiffer much faster when the strain increment size is increased.

In fact, the CS discretization presents an overstiffness with respect to the original formulation. This oversitfness is seen in the zero-incremental results (even at converged values) as well as slightly in the residual-incremental. In the last case, however, the converged values are the same so that the overstiffness can be aleviated with a decrease in strain increment size.

This overstiffness is likely due to how the continuous strain localization tensor $\boldsymbol{B}^{Cont}$ is defined. As can be seen in Equation (4.7), the continuous approach defines this tensor as the elastic one plus a small variation of this tensor, evaluated at the elastic value. Given that second order (and higher) terms are disregarded, this approximation is linear, meaning that with big strain increments the linearized behaviour is made more evident. In the zero-incremental case, disregarding the residual stresses makes the solution more compliant. This, at the same time, provokes that the use of a linear approximation is not that obvious: as seen in the results, the residual-incremental plastic region looks somewhat as a straight line, whereas the zero-incremental presents a curved slope.

5.1.2 Comparison with the residual-incremental formulation when $\Delta\varepsilon \to 0$

The results from 5.1.1 are used again here and compared with the base code. Ideally, both formulations should converge for the same results when the strain increments are approaching zero. Note that this only applies when the residual stress is considered non-zero.

For a very small strain increment, $\Delta\boldsymbol{\varepsilon}_{n+1}$ is very small, so that $\Delta\boldsymbol{\varepsilon}^r_{n+1}$ approaches $\Delta\boldsymbol{\varepsilon}^u_{n+1}$. When this happens, the secant operator $\boldsymbol{C}^{Sr}$ connecting the residual state and the state at time t_{n+1} becomes very close to the elastic operator. Recovering its expression as $\boldsymbol{C}^{Sr} = 3\kappa^{el}\boldsymbol{I}^{vol} + 2\mu^S\boldsymbol{I}^{dev}$ and recalling that the bulk modulus is constant, it is explained why the evaluation of the tensors at the elastic value falls down to evaluating the shear stiffness at elasticity.

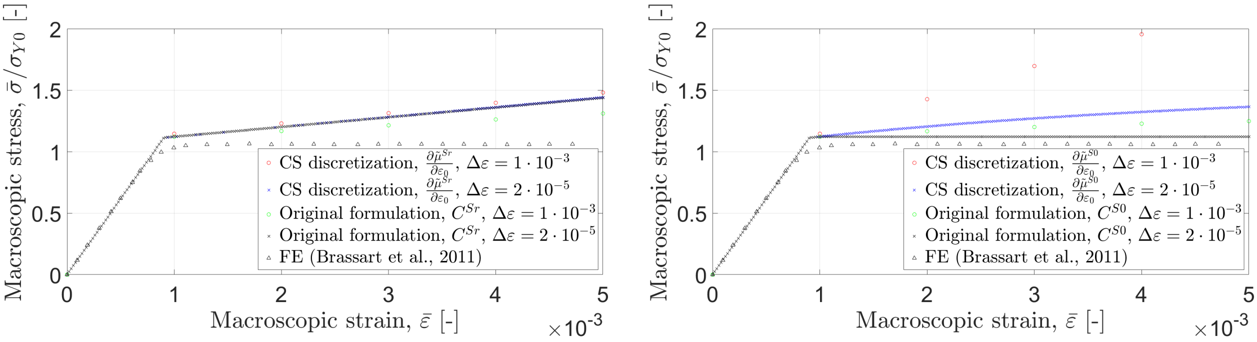

(a) Residual-incremental convergence.

(b) Zero-incremental convergence.

Figure 5.2: Convergence of CS discretization and original formulation with small strain increment.

The curves for $\Delta\varepsilon = 4\cdot 10^{-6}$ have been omitted for simplicity, as they did not add any new information. The curves in Figure 5.2 can be seen to overlap at $\Delta\varepsilon = 2\cdot 10^{-5}$, meaning that they are converging to the same values. For $\Delta\varepsilon = 1\cdot 10^{-3}$, it can be observed that the CS discretization is slightly closer to the curves with finer strain increments, indicating a close convergence at this size.

From these results it is clear that, for an infinitely small strain increment, both formulations will end up converging, therefore confirming the hypothesis first stated of both formulations being equivalent on the limit $\Delta\varepsilon \to 0$.

Note that this only applies to the residual-incremental case. The zero-incremental is a specific case of the residual incremental method, in which the residual stress is purposely set to 0 to increase the compliance of the results. In this specific case, the CS discretization does not mathematically tend to the original code with an infinitesimally small strain increment.

5.1.3 Reduced sensitivity to strain increments

The main advantage of the CS discretization is that results do not change as much with strain increment, when compared with the incremental-secant formulation. This allows for faster computations without losing so much accurracy, saving time. In order to test the accuracy of the results, the code has been tested under a number of strain increments and the results compared. The figure of merit here is once more macroscopic stress, $\bar{\sigma}$. Since now the interest is to increase the size of the strain increment, the values tested go down from the converged value of $\Delta\boldsymbol{\varepsilon} = 1 \cdot 10^{-3}$. The values used now are: $\Delta\varepsilon = 0.02$; 0.01; $4 \cdot 10^{-3}$; $2 \cdot 10^{-3}$ and again $1 \cdot 10^{-3}$. Figure 5.3 showcases the results obtained.

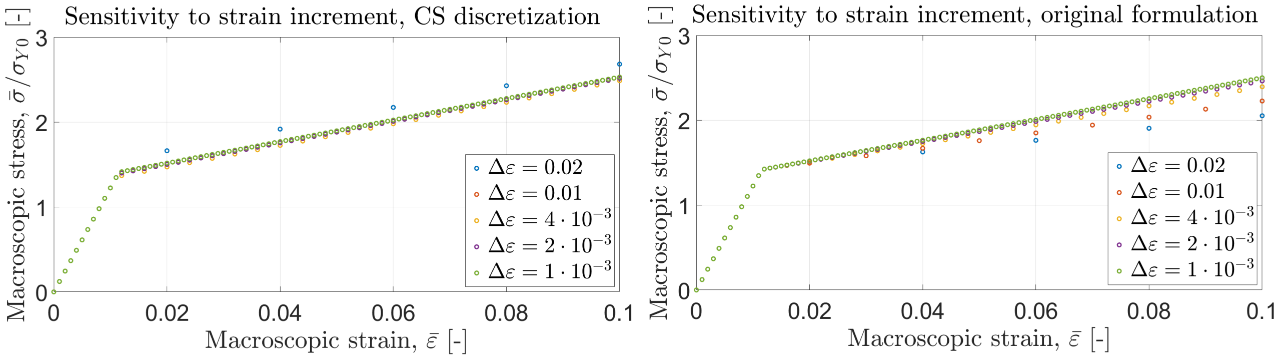

Figure 5.3: Sensitivity to strain increments of the CS discretization. Left shows the CS discretization. The figure on the right, the original formulation,

On the left, except for the 0.02 s line, the rest are very close to each other. In fact, the slope in the plastic region is almost similar on all the cases. This shows how an even bigger strain increment size could be used; as the results on the right can be seen to deviate faster from the converged solution.

For sizes 0.02 and 0.01 in the CS discretization, the results are much stiffer than they should, suggesting an overshooting due to the worse accuracy. When it reaches $4 \cdot 10^{-3}$, it starts slowly becoming stiffer, by converging to the actual solution that has been corroborated with the original formulation.

This improvement is only seen when using the residual-incremental method. For zero-incremental, as explained in 5.1.2, the overstiffness makes the CS discretization results much worse with increasing strain increment size.

5.2 Comparison with the results from [1]

Once the results have been validated and the potential of the new formulation seen in the reduced sensitivity, the final step is to test the cases of the reference paper and see how the CS discretization works with more complex materials. Given the result on the accuracy over the strain increment, the comparisons are performed using $\Delta\varepsilon = 1 \cdot 10^{-3}$.

5.2.1 Case 1

The first case presents an MMC composed by an elastoplastic matrix with continuous fiber inclusions embedded in it. The matrix phase follows the power hardening law $R(p) = kp_0^m$. The properties of each phase are:

Table 5.7: Matrix properties

Matrix properties	
E_0	68.9 GPa
ν_0	0.26
v_0	0.45
σ_{Y0}	95 MPa
k_0	578.25 MPa
m_0	0.529

Table 5.8: Inclusion properties

Inclusion properties	
E_I	344.5 GPa
ν_I	0.26
v_I	0.55
α	∞

Figure 5.4 showcases the results of this case. For the longitudinal loading, both formulations are very close to the FE results. Comparing one method to the other, the CS presents reliable results that are as close to the reference results as the original code. On the transversal case, however, the overstiffness of the CS discretization is very pronounced on the zero-incremental case. The residual-increment, on the other hand, does present results that are closer to the original code, once more slightly overstiff.

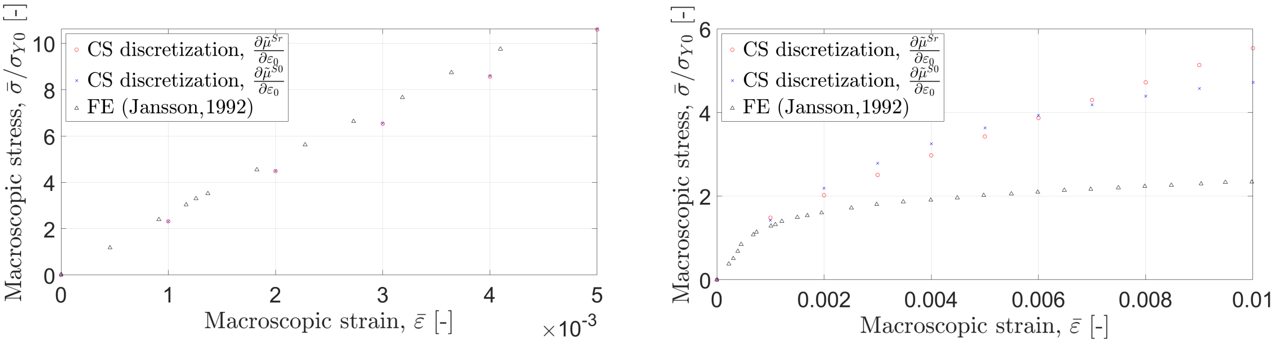

(a) Longitudinal loading.

(b) Transverse loading.

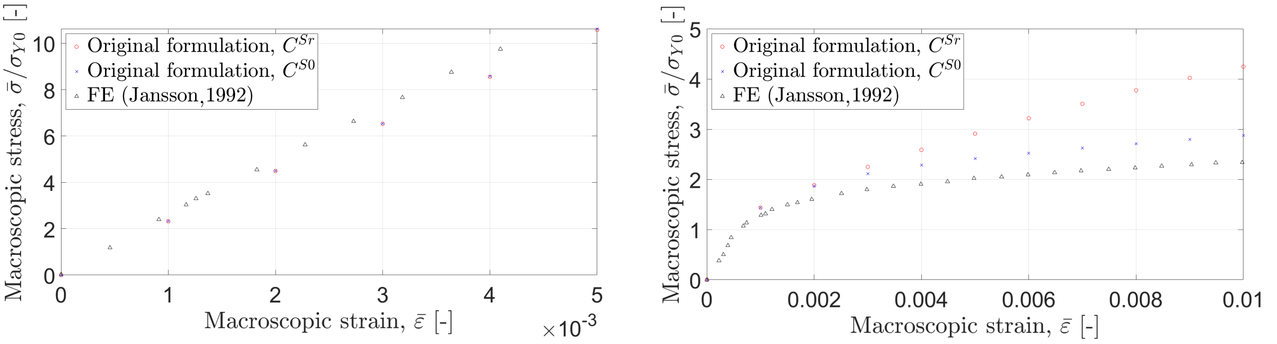

(c) Longitudinal loading.

(d) Transverse loading.

Figure 5.4: Results of case 1. FE from *Jansson* [7].

5.2.2 Case 2

This case is based on a Glass Fibre Reinforced Polymer with short unidirectional, ellipsoidal fibres with $\alpha = 15$. The matrix follows a hardening law $R(p) = k_1 p + k_2(1 - e^{-m_0 p})$.

Table 5.9: Matrix properties

Matrix properties	
E_0	2.1 GPa
ν_0	0.3
v_0	0.843
σ_{Y0}	29 MPa
k_{10}	139 MPa
k_{20}	32.7 MPa
m_0	319.4

Table 5.10: Inclusion properties

Inclusion properties	
E_I	72 GPa
ν_I	0.22
v_I	0.157
α	15

The results of the residual-incremental formulation are once more very similar between CS discretization and the original formulation. This applies to both loadings.

On the zero-incremental case, however, now it is the longitudinal loading that aggravates the differences due to overstiffness.

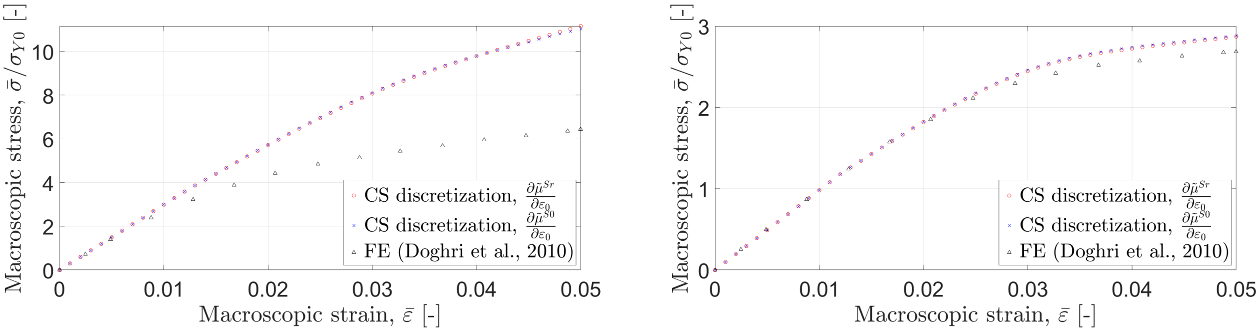

(a) Longitudinal loading.

(b) Transverse loading.

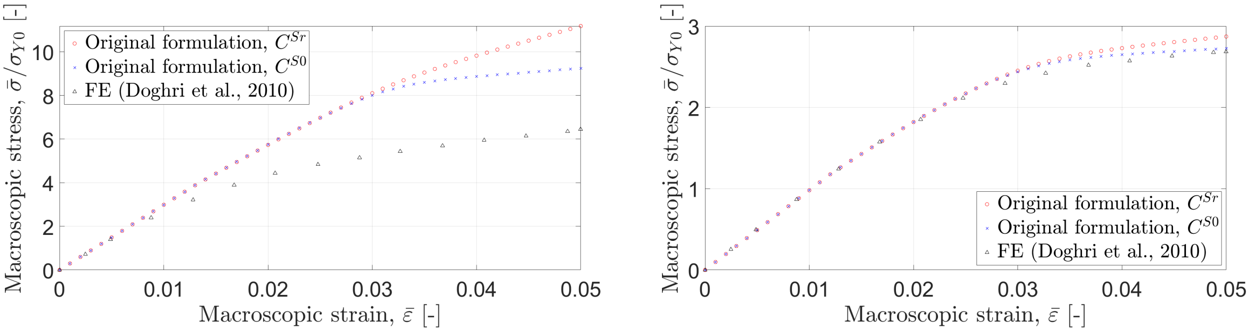

(c) Longitudinal loading.

(d) Transverse loading.

Figure 5.5: Results of case 2. FE from *Doghri et al.* [8].

5.2.3 Case 3

A Glass Fibre Reinforced Polymer with continuous unidirectional fibres. The continuous fibres are represented in the code as spherical inclusions with aspect ratio tending to infinity. The hardening law of the matrix is now $R(p) = k_0(1 - e^{-m_0 p})$.

Table 5.11: Matrix properties

Matrix properties	
E$_0$	2.89 GPa
ν_0	0.3
v_0	0.50
σ_{Y0}	35 MPa
k_0	73 MPa
m_0	60

Table 5.12: Inclusion properties

Inclusion properties	
E$_I$	238 GPa
ν_I	0.3
v_I	0.50

Once more, the results from the CS discretization are overstiff, being the zero-incremental softer than the residual-incremental.

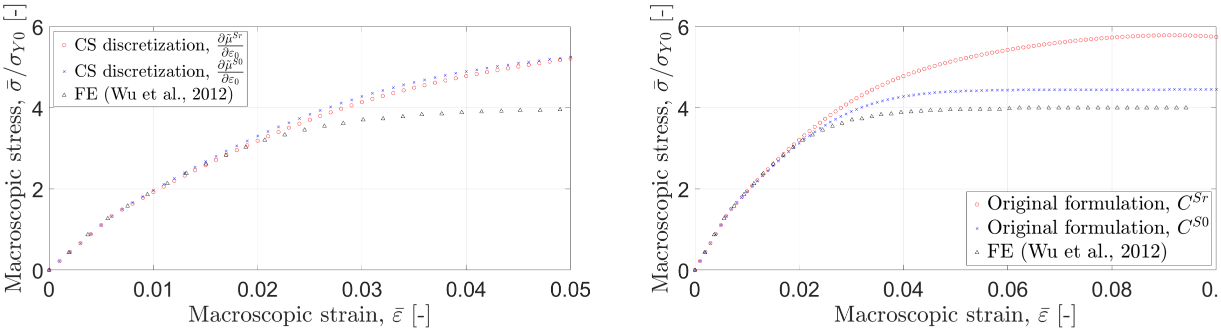

(a) Transverse loading.

(b) Transverse loading.

Figure 5.6: Results of case 3. FE from *Wu et al.* [9].

5.2.4 Case 4

The fourth case is a group of four different MMC's, each with different characteristics.

The first one is a Metal Matrix Composite with spherical inclusions and power hardening law for the matrix: $R(p) = k_0 p_0^m$.

Table 5.13: Matrix properties, MMC 1

Matrix properties	
E$_0$	75 GPa
ν_0	0.3
v_0	0.70
σ_{Y0}	75 MPa
k_0	416 MPa
m_0	0.3895

Table 5.14: Inclusion properties, MMC 1

Inclusion properties	
E$_I$	400 GPa
ν_I	0.2
v_I	0.3
α	1

The second one is a Metal Matrix Composite with spherical inclusions and power hardening law for the matrix. Two cases with $m_0 = 0.05$ and $m_0 = 0.4$ are presented.

Table 5.15: Matrix properties, MMC 2

Matrix properties	
E_0	75 GPa
ν_0	0.3
v_0	0.70
σ_{Y0}	0 MPa
k_0	416 MPa
m_0	0.05 or 0.4

Table 5.16: Inclusion properties, MMC 2

Inclusion properties	
E_I	400 GPa
ν_I	0.25
v_I	0.3
α	3

Following, a Metal Matrix Composite with spherical whiskers and power law hardening is considered:

Table 5.17: Matrix properties, MMC 3

Matrix properties	
E_0	68.89 GPa
ν_0	0.33
v_0	0.868
σ_{Y0}	277.3 MPa
k_0	592.2 MPa
m_0	0.52

Table 5.18: Inclusion properties, MMC 3

Inclusion properties	
E_I	450 GPa
ν_I	0.17
v_I	0.132
α	6.25

Lastly, there is a Metal Matrix Composite with elastic inclusions. Two cases are present, one with spherical inclusions ($\alpha = 1$) and another one with ellipsoidal inclusions ($\alpha = 3$). Once more, power law hardening is assumed for the phase.

Table 5.19: Matrix properties, MMC 4

Matrix properties	
E_0	220 GPa
ν_0	0.3
v_0	0.75
σ_{Y0}	300 MPa
k_0	1130 MPa
m_0	0.31

Table 5.20: Inclusion properties, MMC 4

Inclusion properties	
E_I	200 GPa
ν_I	0.30
v_I	0.25
α	1 or 3

Figures 5.7a through 5.8f show the results for all the MMC's. The testing of the four MMC's shows how the CS discretization handles the different cases presenting feasible results, therefore proving to be quite robust when it comes to the residual-incremental method.

For the zero-incremental, it is very clear that the overstiffness increases with the cases complexity and it is generally not negligible. Furthermore, the fact that it requires more reduction in strain increment size means that this shift of the results is not as easy to correct as it could be in the residual-incremental case.

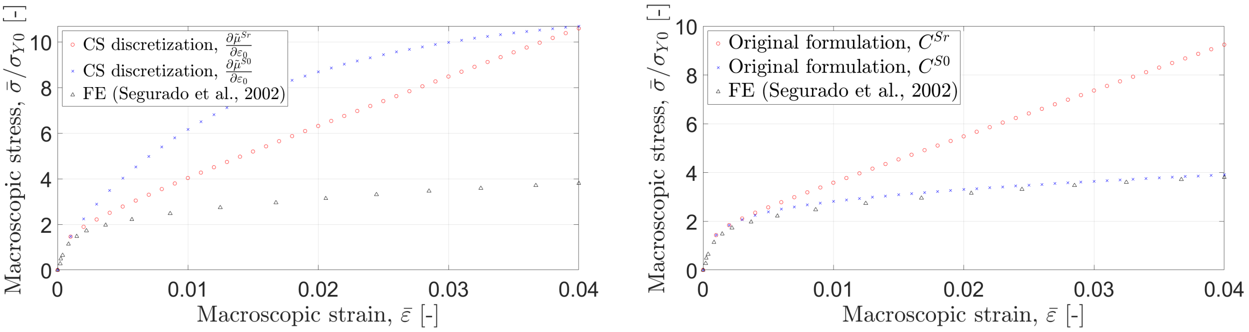

(a) Longitudinal loading. MMC 1.

(b) Longitudinal loading. MMC 1.

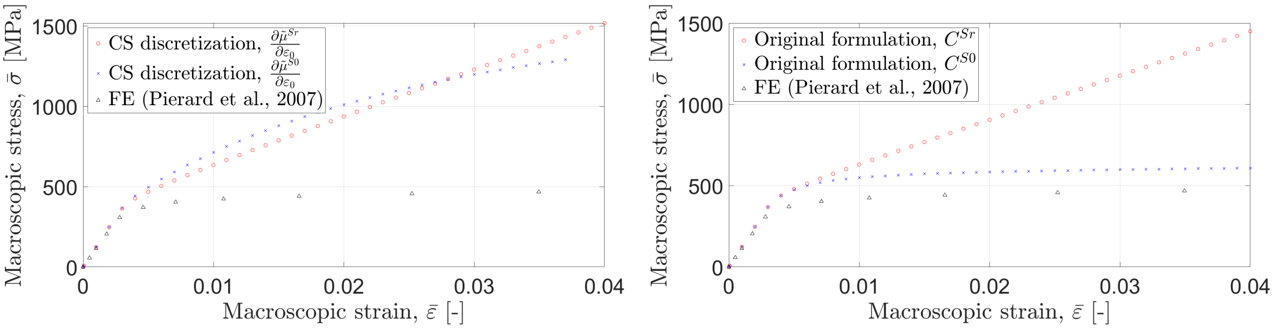

(c) Longitudinal loading. MMC 2, $m_0 = 0.05$.

(d) Longitudinal loading. MMC 2, $m_0 = 0.05$.

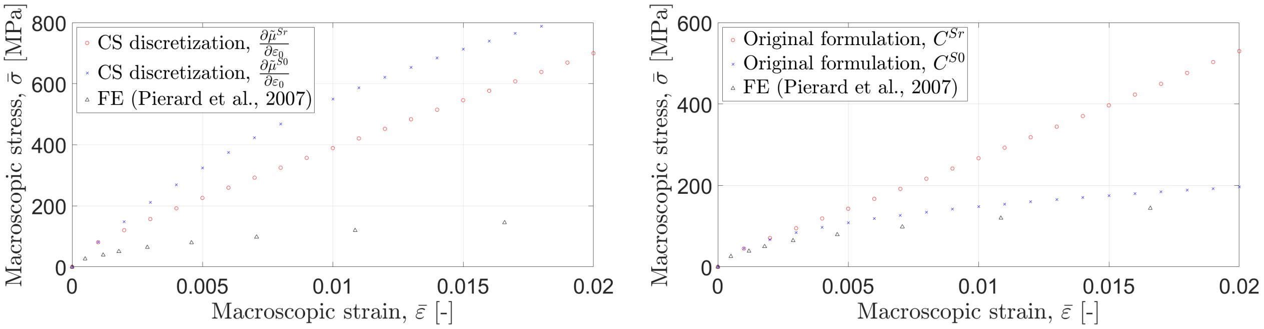

(e) Longitudinal loading. MMC 2, $m_0 = 0.40$.

(f) Longitudinal loading. MMC 2, $m_0 = 0.40$.

Figure 5.7: Results of case 4 (MMC's 1 and 2). FE from *Segurado et al.* [10] and *Pierard et al.* [11].

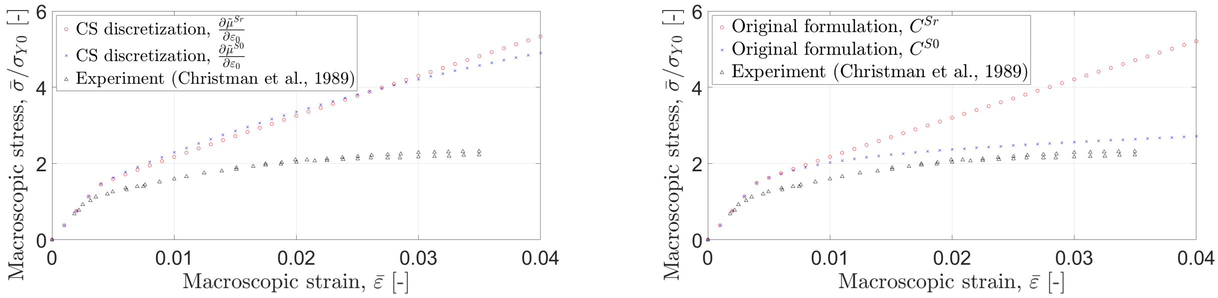

(a) Longitudinal loading. MMC 3.

(b) Longitudinal loading. MMC 3.

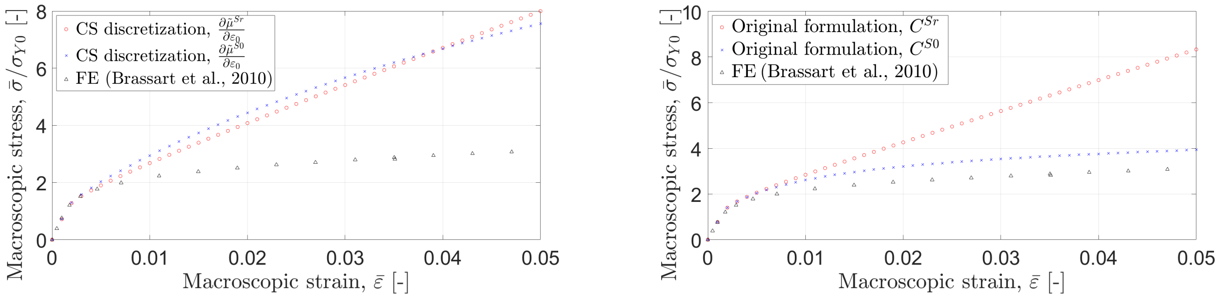

(c) Plane strain tension. MMC 4, $\alpha = 1$.

(d) Plane strain tension. MMC 4, $\alpha = 1$.

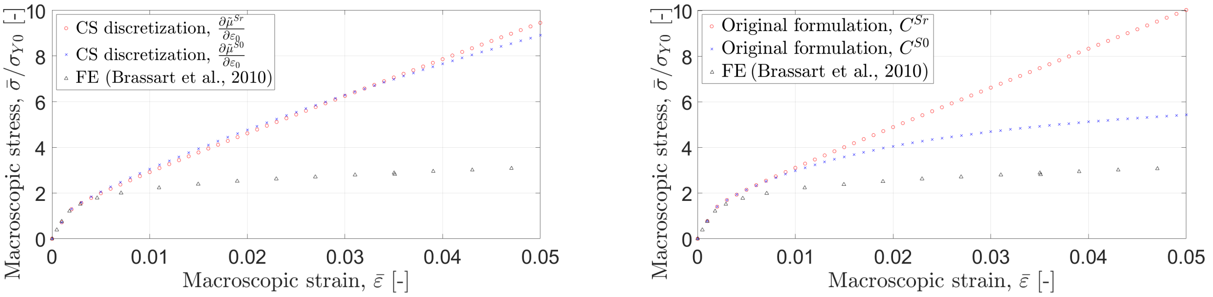

(e) Plane strain tension. MMC 4, $\alpha = 3$.

(f) Plane strain tension. MMC 4, $\alpha = 3$.

Figure 5.8: Results of case 4 (MMC's 3 and 4). FE from *Brassart et al.* [12]. Experimental data from *Christman et al.* [13].

Chapter 6

Conclusions

The development of a new formulation was carried out parting from the incremental-secant formulation developed in [1]. The idea of this continuous formulation was to obtain a new model for the problem that was not based on finite time steps from the beginning. With this, one would in theory be able to use any discretization to switch to finite differences and then use a numerical method of choice to obtain the solutions of the problem. To test this new formulation, a specific discretization, called CS discretization, was implemented and its results compared with the original incremental-secant formulation from the paper.

The results were found to be promising in general. Both formulations have the same results for infinitely small time steps, or equivalently, strain increments for a strain-rate independent model. The new discretization appears to be robust and achieve convergence with a bigger size of the finite increments for the residual-incremental case. The results are not as close to the FE results as the zero-incremental from [1]. However, it does present a way of obtaining accurate first-order moment results in less time. This method could be paired with another one (such as second-order moment methods) to take advantage of the improved computational time that can be achieved with this discretization.

On the other hand, the zero-incremental case presents a less increase in compliance due to the overstiffness that the continuous formulation introduces in the results. Given that second-order terms were dropped in the derivation of $\boldsymbol{B}^{Cont}$, studying if their inclusion could solve this overstiffness problem could be interesting to address this issue.

In conclusion, it was proved that the present method can potentially be modified in the future to obtain quick solutions to be paired with second-order moment methods. The downside of this being, that the zero-incremental method cannot be used to obtain compliant results within a first-order method.

Chapter 7

Future improvements of the method

There are a number of improvements that can be added to the code in the near future. The main ones are:

1. Right now the code only allows the use of elastic inclusions. However, the J_2 plasticity equations are implemented in a generic function. Therefore, the current code could be modified to allow the computation of cases with plasticity in the inclusion phase as well.
2. As mentioned in Section 4.2, the code tested evaluates the unloading strain in the inclusion, for $\boldsymbol{B}^{Cont}$, at time step t_n. Even if this value does not change much, the code could still be improved to have a rigorously fully implicit version by evaluating this value at t_{n+1}.
3. The use of a Crank-Nicholson scheme was also commented by the tutor and advisor; and could be implemented when the previous point is completed.

Lastly, the code can be enhanced to allow the use of the viscoplastic models that are present in the code, therefore expanding even more the materials one could simulate with the new method.

Appendix A

Tensor notation

The frame of continuum mechanics usually requires the use of tensors of different orders. In the present case, second and fourth order tensors are very commonly used, while six order tensors can also appear, but are less frequent.

While more basic mathematics has standardized rules of expressing their different tools, tensors are represented with slight differences depending on the work being read. The purpose of this section is simply to explain the two notations that are used in this paper.

The first and main one, used during most of this project is the bold tensor notation. Tensors are noted with bold symbols, as opposed to scalars which are represented by regular font symbols.

The second one is the index notation, longer but more insightful when it comes to tensor operation. The index notation makes use of arbitrary letters to indicate each of the spatial dimentions of the tensors they are subscripted to. A few examples of equivalences are:

$$\boldsymbol{A} + \boldsymbol{B} = \boldsymbol{C} \qquad ; \qquad A_{ij} + B_{ij} = C_{ij} \tag{A.1}$$

$$\boldsymbol{A} : \boldsymbol{B} = c \qquad ; \qquad A_{ij} B_{ij} = C \tag{A.2}$$

The index notation is also shortened by taking advantage of Einstein's convention. Also, note that the bold notation does not always explicitly state the order of the tensor contraction. For that, the reader must either resort to the index notation or the theory.

The stress and strain fields are represented as second order vectors, i.e., respectively,

$$\boldsymbol{\sigma} \quad \text{or} \quad \{\sigma_{ij}\} \qquad \text{and} \qquad \boldsymbol{\varepsilon} \quad \text{or} \quad \{\varepsilon_{ij}\} \qquad , \tag{A.3}$$

while the operators for the stress-strain relationship are fourth order tensors:

$$\boldsymbol{C} \quad \text{or} \quad \{C_{ijkl}\} \tag{A.4}$$

The rest of the quantities can be can be deduced quickly once these are known. Furthermore, the second order identity tensor is written $\boldsymbol{\delta}$ or $\{\delta_{ij}\}$, while the fourth order identity tensor is represented as $\boldsymbol{I}$ or $\{I_{ijkl}\}$.

Appendix B

Calculation of the Jacobian for the former incremental-secant method

The expression for the Jacobian, $\boldsymbol{J}$, can be obtained from the reference paper, [1]. The definition of the Jacobian is given as:

$$\boldsymbol{J} = \frac{\partial \boldsymbol{F}}{\partial \boldsymbol{\varepsilon}_I} + \frac{\partial \boldsymbol{F}}{\partial \boldsymbol{\varepsilon}_0} : \frac{\partial \boldsymbol{\varepsilon}_0}{\partial \boldsymbol{\varepsilon}_I} \tag{B.1}$$

This results in:

$$\begin{gathered}
\boldsymbol{J} = \boldsymbol{C}^S_{0,n+1} : \left[\boldsymbol{I} - \boldsymbol{S}(\boldsymbol{C}^S_0)^{-1}\right] - \boldsymbol{C}^S_{I,n+1} - \frac{\partial \boldsymbol{C}^S_{I,n+1}}{\partial \boldsymbol{\varepsilon}_I} : \Delta\boldsymbol{\varepsilon}^r_{I,n+1} - \\
\frac{v_I}{v_0}\frac{\partial \boldsymbol{C}^S_{0,n+1}}{\partial \boldsymbol{\varepsilon}_0} : \left[\Delta\boldsymbol{\varepsilon}^r_{I,n+1} - \boldsymbol{S}(\boldsymbol{C}^S_0)^{-1} : \frac{\Delta\boldsymbol{\varepsilon}^r_{I,n+1} - \Delta\bar{\boldsymbol{\varepsilon}}^r_{n+1}}{v_0}\right] - \\
\frac{v_I}{v_0^2}\boldsymbol{C}^S_{0,n+1} \otimes \left(\Delta\boldsymbol{\varepsilon}^r_{I,n+1} - \Delta\bar{\boldsymbol{\varepsilon}}^r_{n+1}\right) :: \left(\boldsymbol{S}(\boldsymbol{C}^S_0)^{-1} \otimes \boldsymbol{S}(\boldsymbol{C}^S_0)^{-1}\right) :: \frac{\partial \boldsymbol{S}}{\partial \boldsymbol{\varepsilon}_0} - \frac{v_I}{v_0}\boldsymbol{C}^S_{0,n+1} : \boldsymbol{S}(\boldsymbol{C}^S_0)^{-1}
\end{gathered} \tag{B.2}$$

The derivatives of the secant operators are also obtained from the reference. A different result is obtained depending on the use of the residual-incremental or the zero-incremental method. For the former, one has

$$\frac{\partial \boldsymbol{C}^{Sr}_r}{\partial \boldsymbol{\varepsilon}_r} = 2\boldsymbol{I}^{dev} \otimes \left[\frac{1}{6\mu^{Sr}_r\left(\Delta\varepsilon^{eq}_r\right)^2}\Delta\boldsymbol{\sigma}_r : \boldsymbol{I}^{dev} : \boldsymbol{C}^{alg}_r - \frac{2}{3}\mu^{Sr}_r\frac{\Delta\boldsymbol{e}_r}{\left(\Delta\varepsilon^{eq}_r\right)^2}\right] \quad , \tag{B.3}$$

while for the zero-incremental, the expression is

$$\frac{\partial \boldsymbol{C}^{S0}_r}{\partial \boldsymbol{\varepsilon}_r} = 2\boldsymbol{I}^{dev} \otimes \left[\frac{1}{6\mu^{0}_r\left(\Delta\varepsilon^{eq}_r\right)^2}\boldsymbol{\sigma}_r : \boldsymbol{I}^{dev} : \boldsymbol{C}^{alg}_r - \frac{2}{3}\mu^{S0}_r\frac{\Delta\boldsymbol{e}_r}{\left(\Delta\varepsilon^{eq}_r\right)^2}\right] \quad , \tag{B.4}$$

Lastly, the term $\Delta \boldsymbol{e} = \boldsymbol{I}^{dev} : \Delta \boldsymbol{\varepsilon}$. Equations (B.3) and (B.4) can be applied to either phase I or 0, applying the corresponding stress and strain tensors and shear stiffness expression.

The phase secant operator can be used to extract the needed information to use in the formulas.

$$\begin{cases} \text{First Lamé parameter, } \lambda = \left(C^S_{r,n+1}\right)_{1,2} \\ \text{Shear stiffness, } \mu = \frac{1}{2}\left(C^S_{r,n+1}\right)_{4,4} \\ \text{Poisson's ratio, } \nu = \frac{\lambda}{2(\lambda+\mu)} \\ \text{Bulk modulus, } \kappa = \lambda + \frac{2}{3}\nu \end{cases} \tag{B.5}$$

The numeric subscripts included on the secant operators indicate that the elements (1,2) and (4,4) of the tensors are used. With these four quantities (along with the inclusion's geometric characteristics, for the correspondent phase), $\boldsymbol{S}$ can be calculated.

Appendix C

Components of the Eshelby tensor and their derivatives

The expression to obtain the Eshelby tensor, $\boldsymbol{S}$, is given component by component by *Wu et al.* in [34]. The base case is considering an inclusion of spheroidal shape. Its lengths along the principal axes 1, 2 and 3, follow $a_1 = a_2 < a_3$. The latter can be divided by each of the other two to define an aspect ratio $\alpha = a_3/a_2 = a_3/a_1$. This aspect ratio serves as a parameter to characterize the inclusion, thus, the expression of the tensor is left as a function of this and the poisson ratio ν.

Note that the Eshelby tensor has been indicated to be a function of the secant operator $\boldsymbol{C}_0^S$. As mentioned, this dependency comes from the use of μ and where it is evaluated. Both here and in Appendix C, μ is not explicit, but its dependency comes through the poisson ratio $\nu = \dfrac{3\kappa - 2\mu}{2(3\kappa + \mu)}$. Again, κ is considered constant due to the volume of the material being so.

The components were already present in the original code and are showcased below:

$$\begin{cases} S_{1111} = S_{2222} = \frac{3}{8(1-\nu)}\left(1 + \frac{1}{\alpha^2-1}\right) + \frac{1}{4(1-\nu)}\left[1 - 2\nu - \frac{9}{4(\alpha^2-1)}\right] g \\ S_{3333} = \frac{1}{2(1-\nu)}\left[4 - 2\nu + \frac{2}{\alpha^2-1} - \left(4 - 2\nu + \frac{3}{\alpha^2-1}\right) g\right] \\ S_{1122} = S_{2211} = \frac{1}{4(1-\nu)}\left[\frac{1}{2} + \frac{1}{2(\alpha^2-1} - \left(4 - 2\nu + \frac{3}{\alpha^2-1}\right) g\right] \\ S_{1133} = S_{2233} = -\frac{1}{2(1-\nu)}\left[\frac{1}{2} + \frac{1}{2(\alpha^2-1)} - \left(1 - 2\nu + \frac{3}{4(\alpha^2-1)}\right) g\right] \\ S_{3311} = S_{3322} = -\frac{1}{2(1-\nu)}\left(1 - 2\nu + \frac{1}{\alpha^2-1}\right) + \frac{1}{2(1-\nu)}\left(1 - 2\nu + \frac{3}{2(\alpha^2-1)}\right) g \\ S_{1212} = \frac{1}{4(1-\nu)}\left[\frac{1}{2} + \frac{1}{2(\alpha^2-1)} + \left(1 - 2\nu - \frac{3}{4(\alpha^2-1)}\right) g\right] \\ S_{1313} = S_{2323} = \frac{1}{4(1-\nu)}\left[-2\nu - \frac{2}{\alpha^2-1} - \frac{1}{2}\left(-2 - 2\nu - \frac{6}{\alpha^2-1}\right) g\right] \end{cases} \tag{C.1}$$

For the rest of the components, a set of symmetries (the minor symmetries) can be used:

$$S_{ijkl} = S_{jikl} = S_{ijlk} \qquad \forall \qquad i,j,k,l = 1,2,3. \tag{C.2}$$

Lastly, g is a function of Poisson's ratio:

$$g = \frac{\alpha}{\left(\alpha^2 - 1\right)^{3/2}} \left[\alpha \left(\alpha^2 - 1\right)^{1/2} - \cosh^{-1}\alpha\right] \tag{C.3}$$

For the particular case in which $\alpha = 1$, the expressions here presented are not valid. Instead, one may use:

$$\begin{cases} S_{1111} = S_{2222} = S_{3333} = \frac{7-5\nu}{15(1-\nu)} \\ S_{1212} = S_{2323} = S_{3131} = 2\frac{4-5\nu}{15(1-\nu)} \\ S_{1122} = S_{2211} = S_{1133} = S_{3311} = \frac{5\nu-1}{15(1-\nu)} \end{cases} \tag{C.4}$$

The same symmetries apply than with the previous expressions.

C.1 Derivative of the Eshelby tensor $\boldsymbol{S}$

The derivative of the Eshelby tensor is useful in the new formulation, since it appears many times in different expressions and derivatives (such as the Jacobian, for example). This appendix shows how these are obtained in a simple manner so that the reader may come back to check the expressions if needed when they are following derivations.

C.2 First derivative

The derivative of the Eshelby tensor, $\dfrac{d\boldsymbol{S}}{d\mu_r^S}$ can be obtained from the components of $\boldsymbol{S}$, given in Appendix C. Since the derivative of $\boldsymbol{S}$ is easier to obtain in terms of Poisson's ratio, the chain rule becomes handy:

$$\frac{d\boldsymbol{S}}{d\mu_r^S} = \frac{d\boldsymbol{S}}{d\nu}\frac{d\nu}{d\mu_r^S} \tag{C.5}$$

Then, the derivative of $\boldsymbol{S}$ with respect to Poisson's ratio can be obtained from the components one by one:

$$\begin{cases} \frac{d\boldsymbol{S}_{1111}}{d\nu} = \frac{d\boldsymbol{S}_{2222}}{d\nu} = \frac{24}{64(1-\nu)^2}\left(1+\frac{1}{\alpha^2-1}\right) + \frac{4}{16(1-\nu)^2}\left[1-\frac{9}{4(\alpha^2-1)}\right] g \\ \frac{d\boldsymbol{S}_{3333}}{d\nu} = \frac{1}{2(1-\nu)^2}\left[2\nu+\frac{2}{\alpha^2-1}-\left(2\nu+\frac{3}{\alpha^2-1}\right) g\right] \\ \frac{d\boldsymbol{S}_{1122}}{d\nu} = \frac{d\boldsymbol{S}_{2211}}{d\nu} = \frac{1}{4(1-\nu)^2}\left[\frac{1}{2}+\frac{1}{2(\alpha^2-1)}+\left(1-\frac{3}{4(\alpha^2-1)}\right) g\right] \\ \frac{d\boldsymbol{S}_{1133}}{d\nu} = \frac{d\boldsymbol{S}_{2233}}{d\nu} = \frac{-1}{4(1-\nu)^2}\left(1+\frac{1}{2(\alpha^2-1)}\right) + \frac{1}{4(1-\nu)^2}\left(4+\frac{3}{\alpha^2-1}\right) g \\ \frac{d\boldsymbol{S}_{3311}}{d\nu} = \frac{d\boldsymbol{S}_{3322}}{d\nu} = \frac{-1}{2(1-\nu)^2}\left(2\nu-3+\frac{1}{\alpha^2-1}\right) + \frac{-1}{2(1-\nu)^2}\left(2\nu-3+\frac{3}{\alpha^2-1}\right) g \\ \frac{d\boldsymbol{S}_{1212}}{d\nu} = \frac{1}{4(1-\nu)}\left[\frac{1}{2}+\frac{1}{2(\alpha^2-1)}+\left(-1-\frac{3}{4(\alpha^2-1)}\right) g\right] \\ \frac{d\boldsymbol{S}_{1313}}{d\nu} = \frac{d\boldsymbol{S}_{2323}}{d\nu} = \frac{1}{4(1-\nu)}\left[-2-\frac{-2}{\alpha^2-1}-\frac{1}{2}\left(-4-\frac{6}{\alpha^2-1}\right) g\right] \end{cases} \tag{C.6}$$

Regarding the missing components, the same symmetries as for the original tensor can be used to obtain them:

$$d\boldsymbol{S}_{ijkl} = d\boldsymbol{S}_{jikl} = d\boldsymbol{S}_{ijlk} \quad \text{for i,j,k,l} = 1,2,3$$

The term $\frac{d\nu}{d\mu_r^S}$ can be evaluated from the expression $\nu = \frac{3\kappa - 2\mu}{2(3\kappa+\mu)}$, which is applicable to the matrix phase since it is isotropic. Furthermore, the bulk modulus of the material, κ, can be assumed to be constant.

$$\frac{d\nu}{d\mu_r^S} = \frac{-9\kappa}{2(3\kappa+\mu_r^S)^2} \tag{C.7}$$

$\frac{d\boldsymbol{S}}{d\mu_r^S}$ is therefore readily obtainable with the chain rule.

The particular case $\alpha = 1$ has a different expression for the derivatives as well.

$$\begin{cases} \frac{d\boldsymbol{S}_{1111}}{d\nu} = \frac{d\boldsymbol{S}_{2222}}{d\nu} = \frac{d\boldsymbol{S}_{3333}}{d\nu} = \frac{2}{15(1-\nu)^2} \\ \frac{d\boldsymbol{S}_{1122}}{d\nu} = \frac{d\boldsymbol{S}_{2211}}{d\nu} = \frac{d\boldsymbol{S}_{1133}}{d\nu} = \frac{d\boldsymbol{S}_{3311}}{d\nu} = \frac{4}{15(1-\nu)^2} \\ \frac{d\boldsymbol{S}_{1212}}{d\nu} = \frac{d\boldsymbol{S}_{2323}}{d\nu} = \frac{d\boldsymbol{S}_{3131}}{d\nu} = \frac{-2}{15(1-\nu)^2} \end{cases} \tag{C.8}$$

C.3 Second derivative

The second derivative, $\frac{d^2\boldsymbol{S}}{d\left(\mu_r^S\right)^2}$, can be obtained from the derivation of the chain rule in Equation (C.5).

$$\frac{d^2\boldsymbol{S}}{d\left(\mu_r^S\right)^2} = \frac{d^2\boldsymbol{S}}{d\nu^2}\left(\frac{d\nu}{d\mu_r^S}\right)^2 + \frac{d\boldsymbol{S}}{d\nu}\frac{d^2\nu}{d\left(\mu_r^S\right)^2} \tag{C.9}$$

$\dfrac{d^2\nu}{d\left(\mu_r^S\right)^2}$ follows from differentiating $\frac{d\nu}{d\mu_r^S}$,

$$\frac{d^2\nu}{d\left(\mu_r^S\right)^2} = \frac{18\kappa}{2(3\kappa+\mu_r^S)^3} \qquad , \tag{C.10}$$

and $\dfrac{d^2\boldsymbol{S}}{d\nu^2}$ can be obtained once more component by component:

$$\begin{cases}
\frac{d^2\boldsymbol{S}_{1111}}{d\nu^2} = \frac{d^2\boldsymbol{S}_{2222}}{d\nu^2} = \frac{3}{4(1-\nu)^3}\left(1+\frac{1}{\alpha^2-1}\right) + \frac{1}{2(1-\nu)^3}\left(1+8\nu-\frac{9}{4(\alpha^2-1)}\right)g \\
\frac{d^2\boldsymbol{S}_{3333}}{d\nu^2} = \frac{1}{(1-\nu)^3}\left[1+\nu+\frac{2}{\alpha^2-1}-\left(1+\nu+\frac{3}{\alpha^2-1}\right)g\right] \\
\frac{d^2\boldsymbol{S}_{1122}}{d\nu^2} = \frac{d^2\boldsymbol{S}_{2211}}{d\nu^2} = \frac{1}{2(1-\nu)^3}\left[\frac{1}{2}+\frac{1}{2(\alpha^2-1)}+\left(1-\frac{3}{4(\alpha^2-1)}\right)g\right] \\
\frac{d^2\boldsymbol{S}_{1133}}{d\nu^2} = \frac{d^2\boldsymbol{S}_{2233}}{d\nu^2} = \frac{-1}{(1-\nu)^3}\left(1+\frac{1}{\alpha^2-1}\right) + \frac{1}{2(1-\nu)^3}\left(4+\frac{3}{\alpha^2-1}\right)g \\
\frac{d^2\boldsymbol{S}_{3311}}{d\nu^2} = \frac{d^2\boldsymbol{S}_{3322}}{d\nu^2} = \frac{-1}{(1-\nu)^3}\left(-2+\nu+\frac{1}{\alpha^2-1}\right) + \frac{1}{(1-\nu)^3}\left(-2+\nu+\frac{3}{2(\alpha^2-1)}\right)g \\
\frac{d^2\boldsymbol{S}_{1212}}{d\nu^2} = \frac{1}{2(1-\nu)^3}\left[\frac{1}{2}+\frac{1}{2(\alpha^2-1)}\left(-1-\frac{3}{4(\alpha^2-1)}\right)g\right] \\
\frac{d^2\boldsymbol{S}_{1313}}{d\nu^2} = \frac{d^2\boldsymbol{S}_{2323}}{d\nu^2} = \frac{1}{2(1-\nu)^3}\left[-2-\frac{2}{\alpha^2-1}+\frac{1}{2}\left(4+\frac{6}{\alpha^2-1}\right)g\right]
\end{cases} \tag{C.11}$$

Here, the missing components can once more be obtained with the minor symmetries. One can then use the chain rule in Equation (C.9) and obtain $\dfrac{d^2\boldsymbol{S}}{d\left(\mu_r^S\right)^2}$.

For the case $\alpha = 1$:

$$\begin{cases}
\frac{d^2\boldsymbol{S}_{1111}}{d\nu^2} = \frac{d^2\boldsymbol{S}_{2222}}{d\nu^2} = \frac{d^2\boldsymbol{S}_{3333}}{d\nu^2} = \frac{4}{15(1-\nu)^3} \\
\frac{d^2\boldsymbol{S}_{1122}}{d\nu^2} = \frac{d^2\boldsymbol{S}_{2211}}{d\nu^2} = \frac{d^2\boldsymbol{S}_{1133}}{d\nu^2} = \frac{d^2\boldsymbol{S}_{3311}}{d\nu^2} = \frac{8}{15(1-\nu)^3} \\
\frac{d^2\boldsymbol{S}_{1212}}{d\nu^2} = \frac{d^2\boldsymbol{S}_{2323}}{d\nu^2} = \frac{d^2\boldsymbol{S}_{3131}}{d\nu^2} = \frac{-4}{15(1-\nu)^3}
\end{cases} \tag{C.12}$$

C.4 Mixed derivative

Lastly, the mixed derivative with respect to the strain, $\dfrac{\partial\left(\frac{d\boldsymbol{S}}{d\mu_r^S}\right)}{\partial\boldsymbol{\varepsilon}}$, is also needed for some computations. It can be obtained from the previous result as:

$$\frac{\partial^2\boldsymbol{S}}{\partial\mu_r^S\partial\boldsymbol{\varepsilon}} = \frac{d^2\boldsymbol{S}}{d\left(\mu_r^S\right)^2}\otimes\frac{\partial\mu_r^S}{\partial\boldsymbol{\varepsilon}} \tag{C.13}$$

Depending on the method being used, Equation (4.16) or (4.12) is used to evaluate this term.

Appendix D

Derivatives of the shear stiffness μ_r^S

This Appendix develops the second derivatives of the shear stiffness for both residual incremental or zero-incremental methods. These magnitudes are required to compute the Jacobian (see Appendix E). Phase subscripts will be omitted for simplicity, since the final result will be applicable to both phases at any time step. The strain or time step subscripts will therefore also be neglected in the appendix. It is understood that all the expressions must be evaluated at the same strain increment (for the current use of the expressions, this is at t_{n+1}). Note that if there is a residual stress, it is considered in the previous strain increment (that is, t_n when the expressions are evaluated at t_{n+1}).

Furthermore, due to the two different definitions of the shear stiffness, two sections are included, one for each formulation.

D.1 Zero-incremental shear stiffness μ_r^{S0}

Differentiating Equation (4.12) once more yields:

$$\frac{\partial^2 \tilde{\mu}^{S0}}{\partial \boldsymbol{\varepsilon}^2} = \frac{12\left(\mu^{el}\right)^4}{\left(\boldsymbol{\sigma}^{tr}\right)^{eq} h}\left[\left(\frac{2}{\left(\boldsymbol{\sigma}^{tr}\right)^{eq}} + \frac{1}{h^2}\frac{d^2R}{dp^2}\right)(\boldsymbol{N}\otimes\boldsymbol{N}) - \frac{3}{2\left(\boldsymbol{\sigma}^{tr}\right)^{eq}}\boldsymbol{I}^{dev}\right] \tag{D.1}$$

D.2 Residual-incremental shear stiffness μ_r^{Sr}

This time, Equation (4.16) is differentiated, since the approximation is the expression needed.

$$\frac{\partial^2 \tilde{\mu}^{Sr}}{\partial \boldsymbol{\varepsilon}^2} = \frac{12\left(\mu^{el}\right)^4}{\left(\Delta\boldsymbol{\sigma}^{tr}\right)^{eq} h}\left[\frac{1}{\left(\Delta\boldsymbol{\sigma}^{tr}\right)^{eq}}(\boldsymbol{N}_m\otimes\boldsymbol{N}) + \left(\frac{2}{\left(\boldsymbol{\sigma}^{tr}\right)^{eq}} + \frac{1}{h_m^2}\frac{d^2R}{dp^2}\right)(\boldsymbol{N}\otimes\boldsymbol{N}) - \frac{3}{2\left(\boldsymbol{\sigma}^{tr}\right)^{eq}}\boldsymbol{I}^{dev}\right] \tag{D.2}$$

Lastly, note that, in the approximation to small strain increments used, $\left(\Delta\boldsymbol{\sigma}^{tr}\right)^{eq}$ approaches the unloading strain as $(\Delta\boldsymbol{\sigma}^u)^{eq}$. This has not been explicited due to them being both equivalent to the expression $\boldsymbol{C}^{el} : \Delta\boldsymbol{\varepsilon}^r$. Indeed, in said limit $\Delta\boldsymbol{\varepsilon}^r \to \Delta\boldsymbol{\varepsilon}^u$.

Appendix E

Calculation of the Jacobian for the proposed formulation

Due to the presence of a good number of sixth order tensors, this section has been written using index notation. This helps clarifying the order of the contractions when several of these tensors are used to operate.

Furthermore, the strain increment notation is also skipped. All the terms depending on time, such as $\Delta\varepsilon_I$ and the shear stiffness and its derivatives, are being evaluated at t_{n+1}.

The equation for the Jacobian written in index notation is:

$$J_{ijkl} = \frac{\partial F_{ij}}{\partial(\varepsilon_I)_{kl}} + \frac{\partial F_{ij}}{\partial(\varepsilon_0)_{mn}} \frac{\partial(\varepsilon_0)_{mn}}{\partial(\varepsilon_I)_{kl}} \tag{E.1}$$

The derivatives of F are obtained as:

$$\begin{cases} \frac{\partial F_{ij}}{\partial(\varepsilon_I)_{kl}} = v_0 \left(\cancelto{0}{\frac{\partial\left(B^{Cont}\right)^{-1}_{ijmn}}{\partial(\varepsilon_0)_{kl}}} (\Delta\varepsilon_I)_{mn} + \left(B^{Cont}\right)^{-1}_{ijmn} \cancelto{I_{ijkl}}{\frac{\partial(\Delta\varepsilon_I)_{mn}}{\partial(\varepsilon_I)_{kl}}} \right) + v_I \cancelto{I_{mnkl}}{\frac{\partial(\Delta\varepsilon_I)_{ij}}{\partial(\varepsilon_I)_{kl}}} - \cancelto{0}{\frac{\partial(\Delta\bar{\varepsilon})_{ij}}{\partial(\varepsilon_I)_{kl}}} \\ \frac{\partial F_{ij}}{\partial(\varepsilon_0)_{kl}} = v_0 \left(\frac{\partial\left(B^{Cont}\right)^{-1}_{ijmn}}{\partial(\varepsilon_0)_{kl}} (\Delta\varepsilon_I)_{mn} + \left(B^{Cont}\right)^{-1}_{ijmn} \cancelto{0}{\frac{\partial(\Delta\varepsilon_I)_{mn}}{\partial(\varepsilon_0)_{kl}}} \right) + v_I \cancelto{0}{\frac{\partial(\Delta\varepsilon_I)_{ij}}{\partial(\varepsilon_0)_{kl}}} - \cancelto{0}{\frac{\partial(\Delta\bar{\varepsilon})_{ij}}{\partial(\varepsilon_0)_{kl}}} \end{cases} \tag{E.2}$$

The terms $\frac{\partial\Delta\bar{\varepsilon}}{\partial\varepsilon_I}$ and $\frac{\partial\Delta\bar{\varepsilon}}{\partial\varepsilon_0}$ are considered 0, since during the Newton-Raphson loop resolution, the strain at composite level is considered constant. It must be noted that this is not the case when computing the algorithmic operator. Furthermore, $\frac{\partial\left(B^{Cont}\right)^{-1}}{\partial\varepsilon_I}$ is only 0 whenever the inclusions phase is considered elastic.

Introducing (E.2) into Equation (E.1) gives:

$$J_{ijkl} = v_0 \left(\left(B^{Cont}\right)^{-1}_{ijkl} + \frac{\partial \left(B^{Cont}\right)^{-1}_{ijmn}}{\partial(\varepsilon_0)_{ab}} (\Delta\varepsilon_I)_{mn} \frac{\partial(\varepsilon_0)_{ab}}{\partial(\varepsilon_I)_{kl}} \right) + v_I I_{ijkl} \tag{E.3}$$

To present the final expression, the term $\dfrac{\partial(\varepsilon_0)}{\partial(\varepsilon_I)}$ at constant $\Delta\bar{\varepsilon}$ can be written as:

$$\frac{\partial(\varepsilon_0)_{ab}}{\partial(\varepsilon_I)_{kl}} = \frac{-v_I}{v_0} I_{abkl} \tag{E.4}$$

Plugging this into Equation (E.3) and reorganizing yields the final expression to be implemented in the code:

$$J_{ijkl} = v_I \left(I_{ijkl} - \frac{\partial \left(B^{Cont}\right)^{-1}_{ijmn}}{\partial(\varepsilon_0)_{kl}} (\Delta\varepsilon_I)_{mn} \right) + v_0 \left(B^{Cont}\right)^{-1}_{ijkl} \tag{E.5}$$

The only term that is not known at this point is the derivative of the new strain localization tensor, this is, $\dfrac{\partial \left(B^{Cont}\right)^{-1}}{\partial(\varepsilon_0)}$. However, one can write

$$\frac{\partial \left(B^{Cont}\right)^{-1}_{ijkl}}{\partial(\varepsilon_0)_{ab}} = - \left(B^{Cont}\right)^{-1}_{ijxy} \frac{\partial \left(B^{Cont}\right)_{xyrs}}{\partial(\varepsilon_0)_{ab}} \left(B^{Cont}\right)^{-1}_{rskl} \qquad , \tag{E.6}$$

so that the term to obtain is now the derivative of the non-inverted strain localization tensor. In order to do this, it can be succesively decomposed into simpler expressions to perform the derivatives on. Starting from Equation (4.7):

$$B^{Cont}_{ijkl} = B_{ijmn}\Big|_{\boldsymbol{C}^{el}_0} H_{mnkl} \tag{E.7}$$

Its derivative is:

$$\frac{\partial \left(B^{Cont}\right)_{ijkl}}{\partial(\varepsilon_0)_{ab}} = \cancelto{0}{\frac{\partial B_{ijmn}\Big|_{\boldsymbol{C}^{el}_0}}{\partial(\varepsilon_0)_{ab}}} H_{mnkl} + B_{ijmn}\Big|_{\boldsymbol{C}^{el}_0} \frac{\partial H_{mnkl}}{\partial(\varepsilon_0)_{ab}} \tag{E.8}$$

Here, $B_{ijmn}\Big|_{\boldsymbol{C}^{el}_0}$ is the strain localization tensor evaluated at the elastic secant operator of the matrix phase, which does not depend on the strain. H, on the other hand, is the expression that multiplies the second term in Equation (4.7). It is defined as:

$$H_{ijkl} = I_{ijkl}$$
$$- \underbrace{\left(\frac{dS}{d\mu_0^S}\Big|_{\boldsymbol{C}_0^{el}} : \left(\left(C_0^{el}\right)^{-1} : C_I^S - I\right) - 2S\Big|_{\boldsymbol{C}_0^{el}} : \left(C_0^{el}\right)^{-1} : I^{dev} : \left(C_0^{el}\right)^{-1} : C_I^S\right)_{ijmn}}_{(E_1)_{ijmn}} \underbrace{: \left(\Delta\varepsilon_I^u \otimes \frac{\partial\tilde{\mu}_0^S}{\partial\varepsilon_0}\right)_{ijmn}}_{(E_2)_{mnkl}}$$

Note that E_1 and E_2 have also been indexed. In fact, these two are the most important expressions since the useful quantity is not H, but its derivative. This can be obtained by using the chain rule as:

$$\frac{\partial H_{ijkl}}{\partial(\varepsilon_0)_{ab}} = -\left(\frac{\partial(E_1)_{ijmn}}{\partial(\varepsilon_0)_{ab}}(E_2)_{mnkl} + (E_1)_{ijmn}\frac{\partial(E_2)_{mnkl}}{\partial(\varepsilon_0)_{ab}}\right) \tag{E.9}$$

For the first term,

$$\frac{\partial(E_1)_{ijkl}}{\partial(\varepsilon_0)_{ab}} = 0 \tag{E.10}$$

The reason behind this is that both the Eshelby tensor S and its derivative $\dfrac{dS}{d\mu_0^S}$ are being already evaluated at the elastic value for the expression of H. This means that they are treated as being constants and thus their derivatives are cancelled, leaving only $(E_1)_{ijmn}\dfrac{\partial(E_2)_{mnkl}}{\partial(\varepsilon_0)_{ab}}$ to be computed.

$$\begin{aligned} \frac{\partial(E_2)_{ijkl}}{\partial(\varepsilon_0)_{ab}} = \frac{\partial\left(\Delta\varepsilon_I^u\frac{\partial\tilde{\mu}_0^S}{\partial\varepsilon_0}\right)_{ijkl}}{\partial(\varepsilon_0)_{ab}} = \cancelto{0}{\frac{\partial(\Delta\varepsilon_I^u)_{ij}}{\partial(\varepsilon_0)_{kl}}}\ \frac{\partial\tilde{\mu}_0^S}{\partial(\varepsilon_0)_{ab}} + (\Delta\varepsilon_I^u)_{ij}\left(\frac{\partial^2\tilde{\mu}_0^S}{\partial\varepsilon_0^2}\right)_{klab} = \\ = (\Delta\varepsilon_I^u)_{ij}\left(\frac{\partial^2\tilde{\mu}_0^S}{\partial\varepsilon_0^2}\right)_{klab} \end{aligned} \tag{E.11}$$

The term $\dfrac{\partial^2\tilde{\mu}_0^S}{\partial\varepsilon_0^2}$ can be evaluated from Equations (D.1) or (D.2), so $\dfrac{\partial E_2}{\partial\varepsilon_0}$ follows directly from above. The derivative of the new strain localization tensor is thus

$$\begin{aligned} \frac{\partial\left(B^{Cont}\right)_{ijkl}}{\partial(\varepsilon_0)_{ab}} = -B_{ijxy}\Big|_{\boldsymbol{C}_0^{el}}\left(\frac{dS}{d\mu_0^S}\Big|_{\boldsymbol{C}_0^{el}} : \left(\left(C_0^{el}\right)^{-1} : C_I^S - I\right) - 2S\Big|_{\boldsymbol{C}_0^{el}} : \left(C_0^{el}\right)^{-1} : I^{dev} : \left(C_0^{el}\right)^{-1} : C_I^S\right)_{xyrs} \\ (\Delta\varepsilon_I^u)_{rs}\left(\frac{\partial^2\tilde{\mu}_0^S}{\partial\varepsilon_0^2}\right)_{klab} \end{aligned}$$

By now, all the elements to compute $\dfrac{\partial\left(B^{Cont}\right)^{-1}}{\partial\boldsymbol{\varepsilon}_0}$ and use it for the Jacobian in Equation (E.5) have been obtained and can be coded.

Bibliography

[1] L. Wu, L. Noels, L. Adam, and I. Doghri. A combined incremental-secant mean-field homogenization scheme with per-phase residual strains for elasto-plastic composites. *International Journal of Plasticity*, 51:80–102, 2013.

[2] Adrian P. Mouritz. *Introduction to aerospace materials.* 2012.

[3] Ir. Michaël Bruyneel. Mechanics of composites. *Course at University of Liège, Aerospace and Mechanical Department*, 2021.

[4] S. Nemat-Nasser and M.Hori. *Applied Mathematics and mechanics.* 1993.

[5] Issam Doghri. *Mechanics of Deformable Solids.*

[6] L. Brassart, L. Stainier, I. Doghri, and L. Delannay. A variational formulation for the incremental homogenization of elasto-plastic composites. *Journal of the Mechanics and Physics of Solids*, 59(12):2455–2475, 2011.

[7] Stefan Jansson. Homogenized nonlinear constitutive properties and local stress concentrations for composites with periodic internal structure. *International Journal of Solids and Structures*, 29(17):2181–2200, 1992.

[8] I. Doghri, L. Adam, and N. Bilger. Mean-field homogenization of elasto-viscoplastic composites based on a general incrementally affine linearization method. *International Journal of Plasticity*, 26(2):219–238, 2010.

[9] L. Wu, L. Noels, L. Adam, and I. Doghri. A multiscale mean-field homogenization method for fiber-reinforced composites with gradient-enhanced damage models. *Computer Methods in Applied Mechanics and Engineering*, 233-236:164–179, 2012.

[10] J. Segurado and J. Llorca. A numerical approximation to the elastic properties of sphere-reinforced composites. *Journal of the Mechanics and Physics of Solids*, 50(10):2107–2121, 2002.

[11] O. Pierard, C. González, J. Segurado, J. LLorca, and I. Doghri. Micromechanics of elasto-plastic materials reinforced with ellipsoidal inclusions. *International Journal of Solids and Structures*, 44(21):6945–6962, 2007.

[12] L. Brassart, I. Doghri, and L. Delannay. Homogenization of elasto-plastic composites coupled with a nonlinear finite element analysis of the equivalent inclusion problem. *International Journal of Solids and Structures*, 47(5):716–729, 2010.

[13] T. Christman, A. Needlemna, and S. Suresh. An experimental and numerical study of deformation in metal-ceramic composites. *Acta metallurgica*, 1989.

[14] Jim Renton, Dennis Olcott, Billy Roeseler, Randy Batzer, Bill Baron, and Alex Velicky. Future of flight vehicle structures (2002-2023). *Journal of Airctaft*, 2004.

[15] Emilie J. Siochi. Graphene in the sky and beyond. *Nature Nanotechnology*, 2014.

[16] J. Fish, P. Nayak, and M.H. Holmes. Microscale reduction error indicators and estimators for a periodic heterogeneous medium. *Computational Mechanics*, 1994.

[17] R. Wentorf, R. Collar, M.S. Shephard, and J.Fish. Automated modeling for complex woven mesostructures. *Computer methods in applied mechanics and engineering*, 1999.

[18] Dr. Roger Assaker, Philippe Hebert, and Dr. Keith Hanna. Enabling the Integrateed Computational Materials Engineering approach.

[19] Huiyu Sun, Shenglin Di, Nog Zhang, Ning Pan, and Changchun Wu. Micromechanics of braided composites via multivariable FEM. *Computers and Structures*, 2003.

[20] I. Doghri and A. Ouaar. Homogenization of two-phase elasto-plastic composite materials and structures study of tangent operators, cyclic plasticity and numerical algorithms. *International Journal of Solids and Structures*, 2002.

[21] P. Kanouté, D.P. Boso, J.L. Chaboche, and B.A. Schrefler. Multiscale Methods for Composites: A Review. *Comput. Methods Eng*, 2009.

[22] J.D. Eshelby. The determination of the elastic field of an ellipsoidal inclusion, and related problems. *Royal Society of London. Series A, Mathematical and Physical Sciences*, 1957.

[23] A. Reuss. Berechnung der Fließgrenze von Mischkristallen auf Grund der Plastizitätsbedingung für Einkristalle. *Zeitschrift für Angewandte Mathematik und Mechanik*, 1889.

[24] W. Voigt. Ueber die Beziehung zwischen den beiden Elasticitätsconstanten isotroper körper. *Annalen der Physik*, 1889.

[25] T. Mori and K. Tanaka. Average stress in matrix and average elastic energy of materials with misfitting inclusions. *Acta Metallurgica*, 1973.

[26] R. von Mises. Mechanics of solid bodies in the plastically-deformable state. 1913.

[27] Somnath Ghosh, Kyunghoon Lee, and Prasanna Raghavan. A multi-level computational model for multi-scale damage analysis in composite and porous materials. *International Journal of Solids and Structures*, 2001.

[28] Jacob Fish and Vladimir Belsky. Multi-grid method for periodic heterogeneous media. Part 2: Multiscale modeling and quality control in multidimensional case. *Computer methods in applied mechanics and engineering*, 1995.

[29] L. Noels. Toward stochastic multi-scale methods in continuum solid mechanics. *Computational and Multiscale Mechanics of Materials, University of Liege, Belgium*, 2020.

[30] Laurence Brassart. Homogenization of elasto-(visco)plastic composites: history-dependent incremental and variational approaches. 2011.

[31] L. Wu, L.Adam, and L. Noels. A micromechanics-based inverse study for stochastic order reduction of elastic UD fiber reinforced composites analyses. *International Journal for Numerical Methods in Engineering*, 2018.

[32] R. Hill. A self-consistent mechanics of composite materials. *J. Mech. Phys. Solids*, 1965.

[33] R. Hill. Elastic properties of reinforced solids: Some theoretical principles. *J. Mech. Phys. Solids*, 1963.

[34] Ling Wu, Laurent Adam, and Ludovic Noels. Micro-mechanics and data-driven based reduced order models for multi-scale analyses of woven composites. *Composite Structures*, 270:114058, 2021.